Review

Graphene Oxide and Reduced Graphene Oxide Saturable Absorbers: Advancements in Erbium-Doped Fiber Lasers for Mode-Locking and Q-Switching

Tahani A. Alrebdi [1,*,†], Noor Fatima [2,3,†], Ali M. Alshehri [4], Adnan Khalil [2] and Haroon Asghar [3,*]

1   Department of Physics, College of Science, Princess Nourah Bint Abdulrahman University, P.O. Box 84428, Riyadh 11671, Saudi Arabia
2   Institute of Physics, Khwaja Fareed University of Engineering and Information Technology, Rahim Yar Khan 64200, Pakistan
3   National Centre for Physics, Quaid-i-Azam University Campus, Islamabad 45320, Pakistan
4   Department of Physics, King Khalid University, P.O. Box 9004, Abha 61413, Saudi Arabia
*   Correspondence: taalrebdi@pnu.edu.sa (T.A.A.); haroon.asghar92@gmail.com (H.A.)
†   These authors contributed equally to this work.

Abstract: Graphene oxide (GO) and reduced graphene oxide (rGO) have emerged as robust materials in the development of SAs for erbium-doped fiber lasers (EDFLs). Their exceptional optical properties, such as broadband absorption and fast recovery times, make them ideal candidates for achieving ultrashort pulse operation in EDFLs. With its higher oxygen content, GO offers greater nonlinearity and a tunable absorption spectrum, while rGO, yielded through chemical reduction, exhibits enhanced electrical conductivity and higher saturable absorption. These properties facilitate the generation of ultrashort pulses in EDFLs, which are highly desired for various medical imaging, telecommunications, and material processing applications. This review paper comprehensively analyzes the advancements in GO and rGO SAs in the context of EDFLs for mode-locking and Q-switching applications. The performance of EDFLs utilizing GO and rGO SAs is critically evaluated, focusing on key parameters, such as modulation depth, pulse duration, repetition rate, average power, pulse energy, peak power, and signal-to-noise ratio. Additionally, this review delves into the various synthesis methods of GO and rGO thin film, highlighting their impact on the optical properties and performance of SAs. The discussion on techniques to integrate the SAs into laser cavities includes direct deposition of nanoparticles/thin-film-based SAs, tapered-fiber-based SAs, and D-shaped SAs. Furthermore, the paper explores the challenges encountered during the fabrication of ideal GO and rGO SAs, with issues related to uniformity, stability, and tunability, along with proposed solutions to address these challenges. The insights provided offer valuable guidance for future research aimed at enhancing the performance of EDFLs using GO/rGO SAs.

Keywords: pulsed laser sources; erbium-doped fiber lasers; Q-switched; mode-locked; GO/rGO saturable absorbers; implementation techniques

1. Introduction

Global connectivity has been enabled through optical fiber, which forms the basis for telecommunication systems in this era of fast-growing technology. Fiber lasers have resulted from advances made in optical fiber technology and are a type of laser that uses an optical fiber doped with rare-earth elements as its active gain medium [1]. Fiber lasers are efficiently pumped by diode lasers, enabling them to generate optical pulses in both continuous-wave (CW) and pulsed modes [2]. The fiber structure has an immense surface area for heat dissipation, resulting in high power output and exceptional beam quality. Consequently, it exhibits remarkable properties, such as low noise, narrow linewidth [3], low cost, ease of fabrication, good directionality, and high efficiency [4]. These properties

provide a vast scope across fiber lasers in numerous fields, including medical, scientific research, and industrial use [3]. However, its main application lies in the telecommunication sector [5]. Figure 1 presents a comprehensive roadmap illustrating the progression of erbium-doped fiber lasers (EDFLs). The roadmap highlights key milestones, from the foundational era of optical fiber innovation to integrating advanced saturable absorbers and current trends shaping the field. This chronological perspective outlines how EDFLs have evolved to meet the demands of modern telecommunications and other applications.
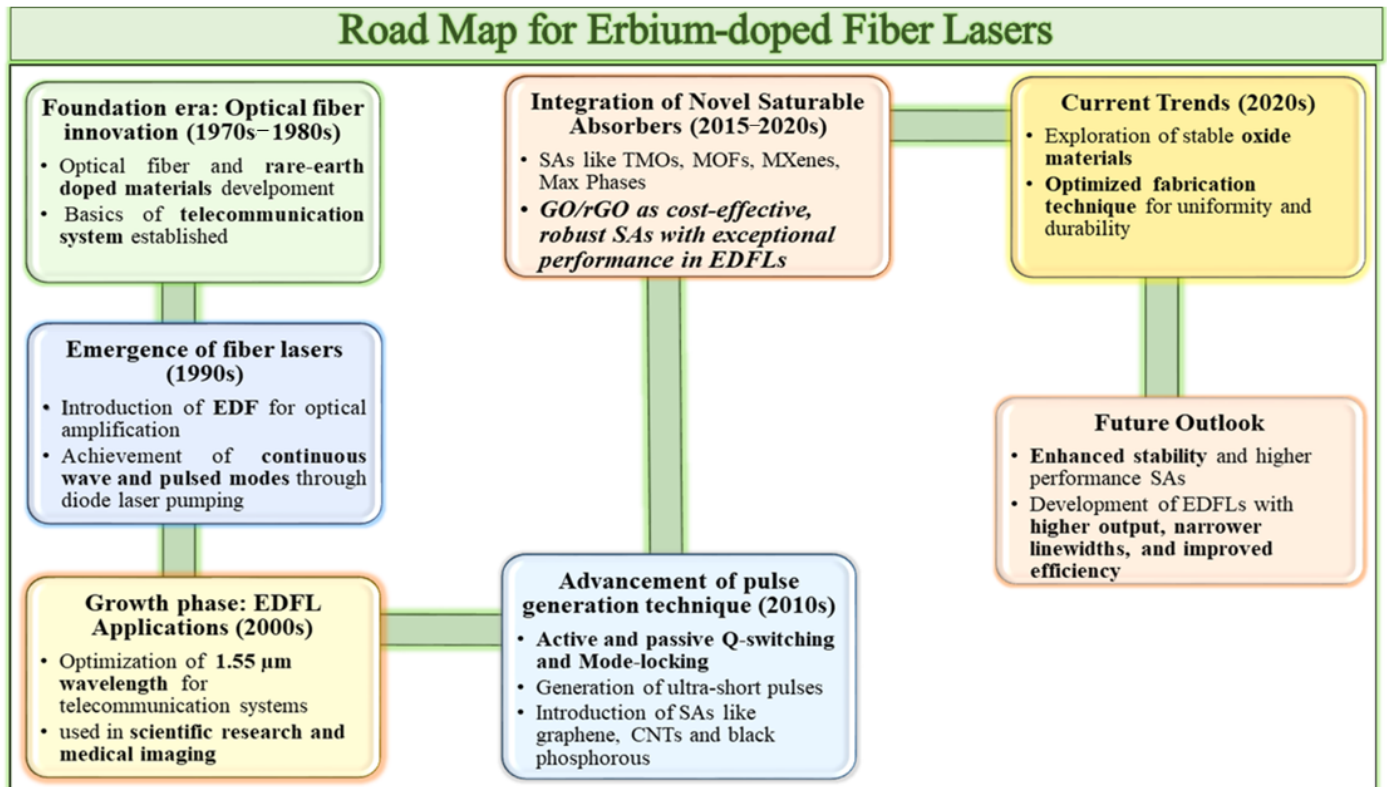
Figure 1. Evolution of EDFLs showing significant advancements in materials, techniques, and applications over time.

Erbium-doped fiber lasers (EDFLs) are among the most extensively applied fiber lasers, and they operate at a wavelength of about 1.55 µm [2]. The wavelength lies within the low-loss band of silica optical fiber, making it suitable for telecommunication systems. The EDFLs function based on stimulated emission within the erbium-doped fiber's core. Erbium ions get excited by pumping through semiconductor diode lasers with wavelengths ranging between 980 and 1480 nm [6]. This excitation causes higher energy levels to be achieved, leading to population inversion. As a result, EDFLs produce both continuous and short-pulse laser emissions at desired wavelengths, which are widely used in many technological fields [7]. Some properties of EDFLs include wider bandwidth, increased gain, and reduced attenuation compared to other types of lasers, besides being cheaper, readily available, and easy to handle or operate [8–10].

EDFLs have a wide range of applications, such as computer links, spacecraft, process control, as well as industrial automation [11]. There are two distinguished ways to achieve ultrashort pulses in EDFLs: Q-switching and mode-locking [12]. In the Q-switching technique, the intra-cavity losses are modulated to cause energy build-up within the cavity, and the modulation is acquired by incorporating the active (modulator) or passive (saturable absorber) component inside the laser cavity [13]. Active Q-switching takes place by introducing an external component, such as a modulator, in the cavity to achieve the desired results. Passive Q-switching involves the addition of SAs or techniques, such as non-polarization rotation, to undergo the phenomenon of Q-switching [14]. Both of these techniques aim to reduce losses

inside the laser cavity and generate ultrashort and ultrafast optical pulses. Simple design, cost-effectiveness, ease of operation, and compactness are properties that lead to a preference for passive Q-switching over active Q-switching [14,15]. The demand for SAs in the domain of EDFLs is widely enhanced, as passive Q-switching bridges the gap between Q-switching and mode-locking. Additionally, mode-locking modifies Q-switching by synchronizing the modes of laser pulses through the addition of an active or passive component inside the laser cavity. This results in the generation of high-power, mode-locked laser pulses emitted with femtosecond pulse durations and repetition rates in a few MHz to hundreds of GHz [13]. In passive Q-switching and mode-locking, the most commonly used SAs include ion-doped crystals [16–22], carbon nanotubes [23–31], black phosphorous [32–38], graphene [39–45], transition metal oxides [46–52], metal-organic frameworks (MOFs) [8,53–58], MXenes [59–65], MAX phase [66–72], transition metal dichalcogenides [73–80], and semiconductor saturable-absorber mirrors (SESAMs) [81–87]. All of these SAs have distinct properties and limitations.

Ion-doped crystals, for instance, exhibit remarkable durability but suffer from limited bandwidth and prolonged relaxation times, constraining their effectiveness [88]. Carbon nanotubes are classified into three distinct categories based on their formation: single-walled (SWCNTs), double-walled (DWCNTs), and multi-walled carbon nanotubes (MWC-NTs). They are widely utilized as SA materials due to their exceptional properties, including a broad absorption range, low saturation intensity, high damage threshold, rapid recovery time, ease of fabrication, and cost-effectiveness [89]. However, high-power laser operation causes thermal degradation of CNTs, thereby limiting their performance as SAs [90]. The direct bandgap of black phosphorous enhances its absorption capabilities, making it ideal for use as an SA in Q-switched and mode-locked EDFLs [36]. However, the instability of BP at ambient temperature limits its performance as an SA [88]. Graphene is one of the remarkable materials discovered for use as a SA to date. Its high electron mobility, large surface area, ultra-broad absorption band, low saturation intensity, and ultrafast recovery time make graphene a superior SA material compared to other 2D materials [91,92]. However, its low modulation depth, significant non-saturable losses, and ability to alter the bandgap are limitations that degrade the performance of graphene as an SA in EDFLs [67,88]. Transition metal di-chalcogenides represent another class of 2D materials deemed suitable as SAs in EDFLs due to their tunable bandgap and high sensitivity to nonlinear responses. However, their relatively weak absorption in the mid-infrared regions renders them incompatible with SAs in mid-infrared lasers [37]. Metal-organic frameworks (MOFs), first synthesized by Yaghi's team in 1999, are classified as semiconductor materials [93]. MOFs are highly suitable for use as SAs due to their remarkable properties, including high tunability, porosity, stability, and large surface area [8]. However, their full potential remains to be explored, particularly in longer wavelength regions [94]. The MAX phases are categorized as nano-laminated materials composed of an early transition metal (M), an A-group element (A), and C, N, B, and P (X) [95]. These materials are highly regarded for their potential as SAs due to distinctive attributes, such as high electrical conductivity, stability, exceptional mechanical strength, and outstanding oxidation resistance. However, further exploration of their performance in the near-infrared spectrum is crucial [68]. MAX phases can undergo acid etching to selectively remove aluminum layers, resulting in the formation of MXenes (Mn + 1Xn), composed of transition metals and carbon or nitrogen. MXenes exhibit high saturable absorption, enhanced modulation depth, tunable bandgap, and effective electron density, making them promising SAs in EDFLs [62]. However, despite their excellent properties, MXenes face challenges due to their complex fabrication processes and environmental instability [96]. Transition metal oxides, such as zinc oxide (ZnO), are popular choices for SAs due to their exceptional electrical and optical properties. However, when integrated into fiber laser ring cavities, TMOs such as ZnO present several drawbacks, including lower stability, reduced damage threshold, and sensitivity to environmental conditions [97]. SESAMs are favored in ultrafast lasers due to their low saturation intensity and high modulation depth. However, they are also subject to performance limitations, such as complex fabrication methodologies and a

narrow operating wavelength range [98]. So, still, there is a huge demand for an optimal SA that encompasses enduring stability over extended periods, resilience to high optical intensities, rapid recovery rates, minimal saturation intensity, optimal modulation depth, and straightforward fabrication and integration within laser cavities [99].

Oxide materials offer exciting possibilities in the field of pulsed laser sources due to their exceptional properties as SAs. The general advantages of oxide-material-based SAs include broadband absorption and fast recovery times [100–103]. These materials are integral in generating pulses, which rely on saturable absorption to achieve short, intense pulses of light. The fast recovery times of oxide materials are crucial, as they enable rapid re-absorption of the laser light after saturation, thereby allowing for generating high-repetition-rate pulses. This fast response contributes significantly to the overall efficiency and performance of the laser system. The nonlinear optical properties of oxides further enhance their role as SAs [104]. These properties allow for the modulation of light intensity in a manner that supports the generation of ultrashort pulses with precise control over the pulse duration and energy. Additionally, the broad spectrum of optical properties and applications makes oxides highly suitable for advanced optical technologies. EDFLs demand SAs with bandgaps compatible with their operating wavelength of 1550 nm in the near-infrared (NIR) region to generate ultrashort laser pulses [2]. Tunable bandgaps of oxide nanomaterials offer to support EDFLs by working at their operating wavelengths to produce the desired output. These excellent attributes of oxide nanomaterials make them suitable for approaching various critical requirements in laser systems, including damage resistance, optical modulation capabilities, and stability. This discussion outlines the saturable absorption properties, tunability of bandgaps, and nonlinear character of oxides, making them highly adaptable and compatible to work as SA in EDFLs.

Graphene oxide (GO) and reduced graphene oxide (rGO) have gained significant attention as SAs in EDFLs due to their unique optical properties [105]. Graphene oxide (GO), the graphene precursor, is a well-known oxide material with a unique structure consisting of sp^3 hybridized carbon atoms bonded with oxygen atoms. Reduced graphene oxide (rGO) comprises graphene-like sheets prepared by removing the oxygen-containing groups from graphene oxide [106]. GO/rGO materials exhibit broadband absorption, ultrafast recovery times, and high damage thresholds, making them ideal candidates for mode-locking and Q-switching in fiber lasers [107,108]. The two-dimensional (2D) structure of GO and rGO allows for strong light–matter interactions, enhancing their nonlinear optical properties, such as saturable absorption, which is essential for generating ultrashort pulses in EDFLs. Additionally, the tunability of rGO's optical properties through controlled reduction of GO enables precise adjustment of its absorption characteristics, offering flexibility in laser design. Compared to traditional SAs, such as SESAMs, GO and rGO are cost-effective, easy to fabricate, and can be integrated into fiber laser systems without requiring complex alignment or packaging. This simplicity, combined with their ability to operate at the telecommunication wavelength of 1.55 μm (erbium's emission range), makes them particularly attractive for ultrafast photonics applications, setting them apart from other advanced SAs [109]. Moreover, rGO's better conductivity and improved optical transparency compared to GO further enhance its performance as an SA. Due to the unique physical or chemical properties of the GO/rGO as SAs, compared to the traditional SAs mentioned above, extensive research has explored their application in Q-switched and mode-locked EDFLs. However, a comprehensive review covering the nonlinear optical properties, fabrication techniques, and implementation strategies of GO/rGO SAs, as well as their impact on pulse parameters, is still lacking. This review bridges this gap by presenting a detailed analysis that provides a clearer understanding of the role of GO/rGO SAs and their contribution to the field of EDFLs through the critical discussion of advancements and challenges. Here, we review the performance of Q-switched and mode-locked EDFLs using GO/rGO as SAs, showcasing their exceptional nonlinear optical properties in pulsed fiber lasers. The characteristics of EDFLs based on the GO/rGO nanomaterial SAs, including their modulation depth, pulse duration, repetition rates,

average output power, and signal-to-noise ratio (SNR), are compared and summarized. Additionally, the techniques utilized to prepare and implement SAs inside the laser cavity are further explored.

The paper is structured as follows: In Section 2, the structure, synthesis and nonlinear optical characteristics of GO/rGO-based SAs are described. The implementation techniques of prepared SAs using direct deposition of nanoparticles/thin film, tapered fiber, and D-shaping inside the EDFL cavity are discussed in Section 3. Further discussions on the performance of Q-switched and mode-locked EDFLs subject to GO/rGO SAs are presented in Section 4.

2. Structure, Synthesis, and Nonlinear Characteristics of GO/rGO Nanostructures

2.1. Structure of GO/rGO Nanostructures

GO is a 2D material derived from graphene, characterized by its sheet-like structure composed of carbon atoms arranged in a hexagonal lattice. The presence of various functional groups, such as hydroxyl, epoxy, and carboxyl groups, disrupts the pristine graphene lattice, introducing oxygen atoms into the structure and leading to increased defect density and altered electronic properties. This functionalization enhances GO's hydrophilicity and makes it dispersible in aqueous solutions, facilitating its use in various applications, including sensors, composites, and energy storage devices [110]. In contrast, reduced rGO is produced through the reduction of GO, which restores some of the graphene's sp^2 hybridization, resulting in a structure that is closer to that of pristine graphene. This reduction process can be achieved through thermal, chemical, or electrochemical methods, effectively decreasing the oxygen content and restoring electrical conductivity, though rGO often retains some oxygen functionalities, leading to a heterogeneous structure with varying degrees of reduction [111]. The atomic arrangement of rGO consists of a similar hexagonal lattice, but the presence of residual functional groups can lead to disruptions in the ideal structure, influencing its mechanical, electrical, and thermal properties, thereby affecting its performance in applications, such as flexible electronics and energy devices [112]. Although GO offers higher dispersibility than rGO, still rGO is preferred due to its better thermal and electrical properties, resulting from the reduction of oxygen groups. Additionally, GO and rGO exhibit excellent saturable absorption character and ultrafast relaxation times [112], making them suitable to serve as SAs in EDFLs [106]. Moreover, a relatively simple and cost-effective synthesis techniques increases the worth of GO and rGO to be used as SAs [113].

2.2. Synthesis of GO/rGO Nanostructures

Hummer's method and the modified Hummer's method are considered to be simple and economical methods for the preparation of high-quality GO/rGO thin film [114]. These techniques utilize string-oxidizing agents in the presence of sulfuric oxide to oxidize graphite and fabricate GO and rGO nanostructures. The modified Hummer's method is a modification of Hummer's method that aims to reduce the toxicity and reaction time, along with controlling oxidation levels by the addition of various reactant agents and temperature control adjustments. The oxidation of graphite flakes is achieved by adding oxidizing agents, i.e., potassium permanganate ($KMnO_4$) in the solution of sulfuric acid (H_2SO_4) and sodium nitrate ($NaNO_3$), followed by continuous stirring. The GO suspension achieved by washing the mixture is filtered, washed, and dried to achieve GO with pH maintained at 4 and 5 for further use [112]. A schematic diagram of the synthesis of GO using the Hummer's method technique is shown in Figure 2.

The schematic diagram of the synthesis of rGO using the modified Hummer's method technique is shown in Figure 3. The modified Hummer's method uses a sulfuric-phosphoric acid mixture instead of sodium nitrate, which provides enhanced control over oxidation levels, reduction of toxicity, and operation at room temperature, compared to Hummer's method [115]. The rGO is further prepared by the elimination of oxide groups from GO, typically via a thermal reduction method, as reported by Li et al. [116]. The GO and rGO

thin films are prepared by dissolving them in a compatible polymer, i.e., polyvinyl alcohol (PVA), followed by stirring and drying, as reported by Mat et al. [113]. The prepared thin films are then integrated into fiber ferrules [117–121], tapered fiber [109], and D-shaped fiber [122,123] to act as an SA in the EDFL cavity.
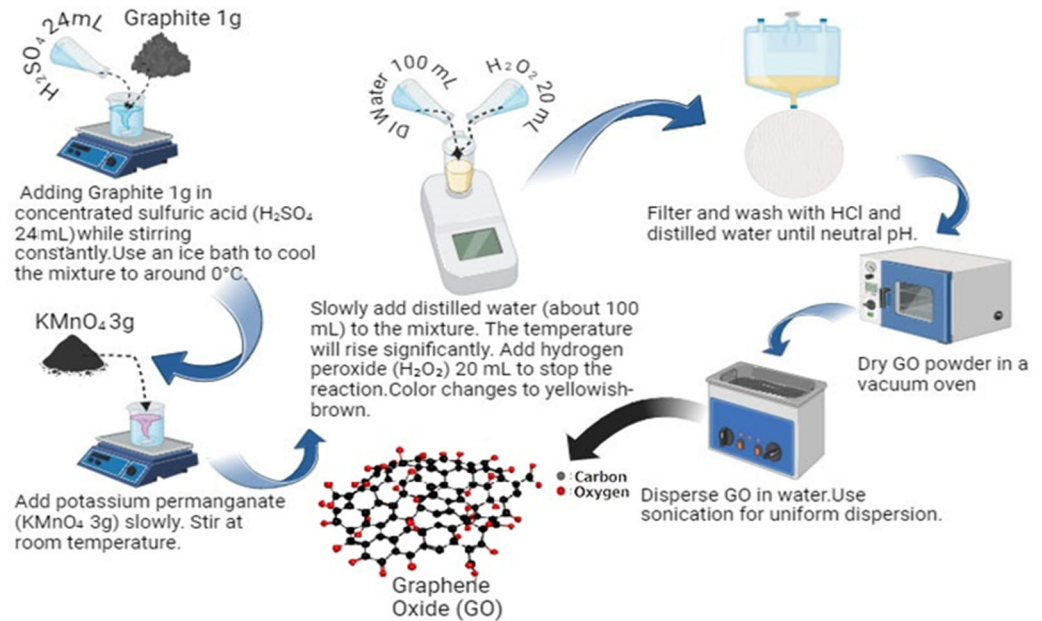

Figure 2. Schematic diagram of the synthesis of GO using the Hummer's method technique.
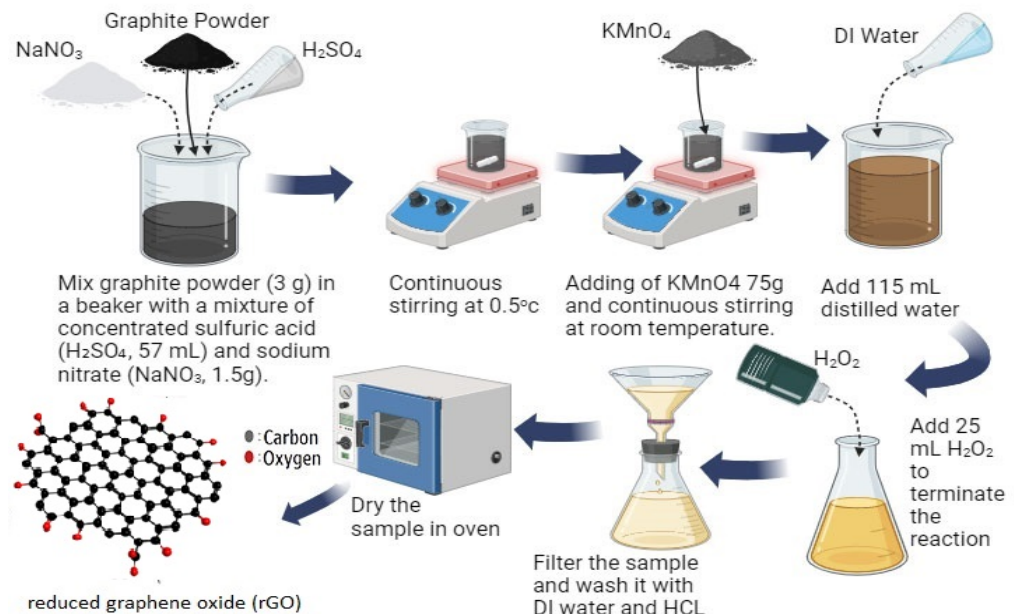

Figure 3. Schematic diagram of the synthesis of rGO using the modified Hummer's method technique.

The concentration of oxidizing agents and acids must be controlled and added precisely in both the Hummer and modified Hummer's methods to ensure the preparation of GO with efficient oxidation and intercalation. The disturbance in the quantity or reaction time of any agent can cause impurity and irregularity in the GO structure that would hinder its performance as an SA by negatively impacting its nonlinear properties. The control over the temperature is specifically required in Hummer's method to ensure smooth oxidation. The transition from a low temperature of 5 °C to a high temperature of 30 °C

must take place smoothly to avoid any unwanted reaction or thermal decomposition to achieve uniform oxidation of graphite.

Alongside the careful synthesis of GO/rGO, the size and form of the sample play a critical role in determining their impact as SAs in Q-switched and mode-locked EDFLs. Typically, the thin films of GO/rGO SAs are integrated into the EDFL cavity. Saha et al. investigated the impact of non-uniformity and wrinkling of the thin film via a mode-locking phenomenon, which presented valuable results [124]. The thinner films with the size of imperfection exceeding the critical limit are preferred for mode-locking due to their ability to balance between a fast recovery time and optimal modulation depth. This balance is critical for generating stable mode-locked pulses. Conversely, relatively thicker films are preferred for Q-switching to yield a high modulation depth and enhance the ability to control energy storage before saturation. These results depict the importance of the optimal size of the active area and thickness of GO/rGO layers, as they impact many critical factors, such as the recovery time, saturation intensity, and insertion losses, to achieve desired pulse characteristics.

2.3. Nonlinear Characteristics of GO/rGO Nanostructures

It has been noticed that the Hummer and modified Hummer's methods strongly influence the nonlinear optical properties of GO and rGO by altering their structural, electrical, and optical properties, which significantly impacts their performance as SAs in EDFLs. Raman spectroscopy is crucial for examining the structural and electrical properties of GO and rGO, due to their significant impact on their nonlinear optical properties as SAs [125]. The Raman spectrum depicts D (~1340 cm^{-1}) and G (~1574 cm^{-1}) bands that symbolize the structural defects and sp^2 carbon atoms, respectively [126]. GO prepared by the modified Hummer's method exhibits a disordered structure due to the introduction of abundant oxygen-containing functional groups, such as hydroxyl, epoxy, and carboxyl groups, via reduction, which is confirmed by Raman spectroscopy, as reported by Sobon et al. [115]. These structural defects enhance the bandgap of GO, along with the introduction of localized states within the bandgap. These defects also act as scattering centers, influencing light transmission and saturable absorption efficiency. It allows the GO to play the role of an optical limiter and somehow limits its saturable absorption ability. So, the removal of oxygen-containing groups by laser, chemical, or thermal reduction restores the partial conjugation of GO by converting it to rGO [115]. The re-establishment of π-π conjugation on rGO leads to a reduced bandgap and efficient saturable absorption at higher intensities, making it highly compatible to generate short pulses.

Scanning electron microscopy (SEM) is used to analyze the structural transformations and surface morphology of GO and rGO [125]. GO possesses a wrinkled, layered structure due to oxygen-rich groups. It enhances the interlayer spacing, which directly impacts the light transmission and saturable absorption efficiency of GO [126]. Removal of oxygen groups from rGO restores its partial conjugation structure, retaining a compact and graphitic form, and enhancing its nonlinear character and performance as an SA in EDFLs [126]. X-ray photoelectron spectroscopy (XPS) is another essential tool to assess the reduction efficiency of GO and rGO through the chemical state and elemental composition [125]. It reveals the carbon and oxygen peaks of GO, indicating the density of carbon–oxygen bonds, while XPS of rGO reveals decreased oxygen content with an enhanced C/O ratio, indicating the successful restoration of sp^2 carbon networks. This restoration influences the saturable absorption efficiency to generate ultrafast and stable pulses [125]. The Z-scan technique reveals the nonlinear optical parameters of GO and rGO, such as modulation depth, saturation intensity, etc., further confirming their potential to generate short pulses [107]. These techniques reveal that structural and morphological changes induced during preparation heavily affect the modulation depth of GO and rGO. The defects and absence of a fully conjugated structure due to the introduction of oxygen-containing groups and disruption of the sp^2 carbon network limits the ability of GO to transit from a high absorption state to a low absorption state under high light

intensities, causing low modulation depth values. However, the modulation depth of rGO is considerably high due to the restoration of the sp^2 network, which directly influences the higher repetition rate and pulse stability in EDFLs. Along with structural changes, the optimized number of layers of nanomaterials is another crucial parameter for optimizing the modulation depth, as it also contributes to the transition of states under light intensities. On the other hand, excessive layering may lead to enhanced scattering losses, limiting pulse operation. This discussion strongly proves GO and rGO's ability to generate ultrashort pulses from EDFLs with high efficiency, which has already been investigated and reported in many papers [109,114,127–131].

The Raman spectroscopy, SEM, Z-scan, and XPS results provide a comprehensive understanding of structural, chemical, nonlinear optical, and morphological characteristics of GO and rGO, directly justifying their ability to act as SAs and correlating their applications in high-power laser systems.

The use of machine learning and deep learning to further study the nonlinear optical properties of the GO/rGO materials, such as defects and structure, can broaden the view and provide deep insight for new horizons. It can be achieved by analyzing large datasets to detect complicated patterns and optimize the synthesis of GO/rGO SAs, resulting in enhanced and stable pulse generation in EDFLs and high-power laser systems [132].

3. Techniques Employed for GO/rGO SAs' Implementation in the Laser Cavity

Several techniques have been employed to incorporate GO/rGO SAs inside a laser cavity, each optimized for different lasers and desired performance characteristics. The most common technique involves the incorporation of thin films, nanoparticles, tapered fibers, and D-shaped fibers within the laser cavity. These prepared GO/rGO SAs can be placed in a position on the fiber ferrule, where they interact with the intra-cavity laser beam. A detailed description of various techniques utilized for the deposition of SAs upon fiber ferrules and then implemented inside the laser cavity is presented below.

3.1. Direct Deposition of Nanoparticles and Thin-Film-Based SAs on Fiber Ferrules

Fiber ferrules in fiber lasers are widely used to incorporate the SAs in the EDFL cavity by placing or embedding them at the interface where fibers are spliced or connected via FC/PC connectors. The GO/rGO SAs are typically deposited on fiber ferrules as thin films, or nanoparticles, ensuring the direct passage or interaction of light through the SA layer. The physical contact between the two fiber ferrules, along with SA occurring through index-matching gel [113,118,133], offers a reduced reflection that leads to enhanced saturable absorption efficiency [118]. The schematic diagrams of direct deposition of GO nanoparticles and GO thin film on the fiber ferrule are shown in Figure 4a,b and Figure 5a,b, respectively. This facilitates an effective light–matter interaction, leading to enhanced saturable absorption and to modulation of the laser output intensity. Various techniques are utilized to deposit the oxide SA thin film upon fiber ferrules, some of which are discussed below.

The spray-coating method is a straightforward and inexpensive method that involves the sonication of oxide SA to undergo atomization [134]. These atomized droplets are sprayed upon the ferrules to form a uniform coating. Monteiro et al. reported the deposition of graphene oxide SA at the end of the fiber connector through the spray-coating method [117]. The sonication of the GO layer with 95% monolayer content played a critical role in improving the homogeneity of the GO layer, which enhances the overall quality and optical properties of the SA layer when integrated into the EDFL system through fiber ferrules. However, the risk of loss of GO material is enhanced by this approach, as a large amount of spray does not interact with the ferrule's surface [135].
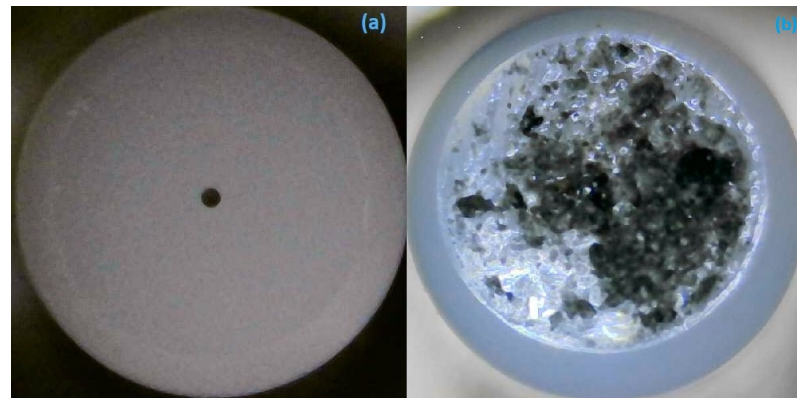
Figure 4. (**a**) Fiber ferrule without SA deposition. (**b**) Fiber ferrule with GO nanoparticle-based SA.
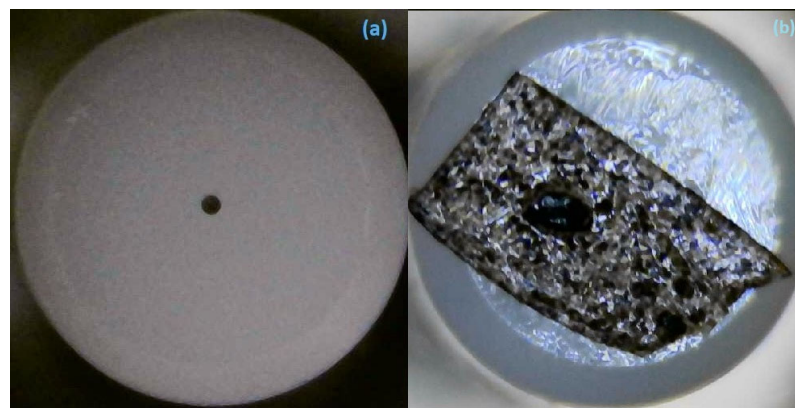
Figure 5. (**a**) Fiber ferrule without SA deposition. (**b**) Fiber ferrule with GO thin-film-based SA.

Optical deposition is another innovative method, which utilizes laser operation to deposit oxide SA onto the ferrule. Yap et al. investigated the deposition of reduced graphene oxide (rGO) SA onto the fiber ferrule using the optical deposition method [106]. The fiber end submerged in rGO solution was exposed to a 980 nm laser for 40 min to ensure the uniform and targeted deposition of rGO SA onto the ferrule. The controlled laser power and deposition time offer fine-tuning of the SA optical character along the optimized interaction among the rGO SA and laser light in the fiber core. So, this highly targeted approach is considered an optimal method for oxide SA deposition upon fiber ferrules. However, this method faces the challenge of achieving consistent deposition over large areas, which reduces its scalability [91].

Depositing SAs directly onto the fiber ferrule in the form of nanoparticles or a thin film in EDFLs offers several advantages. First, this configuration simplifies the laser cavity by eliminating the need for complex free-space alignment or bulky components, making the design more compact and easier to implement. Moreover, by using nanoparticles or thin films, the GO/rGO SAs provide better control over the pulse characteristics, as it allows precise tuning of the SA deposited on the fiber core. Additionally, direct deposition techniques enable cost-effective manufacturing and allow for integration with a variety of SA materials, such as graphene or carbon nanotubes, to achieve different operating wavelengths and pulse durations, thus expanding the versatility and performance of EDFLs [136]. Along with the advantages, the direct deposition of SA on the fiber ferrules requires the careful and uniform deposition of SA to avoid damage or localized losses. Additionally, in high-power fiber lasers, thermal disturbances in SAs can induce thermal lensing, which disrupts the pulse stability and may cause damage to the optical components in high-power applications [137].

3.2. Tapered-Fiber-Based SAs

Tapered fibers are optical fibers that are narrowed at the center or edge through a heat and pulling process by reducing the fiber diameter [138]. GO/rGO SAs are coated on the surface of the tapered fiber to allow a stronger interaction between the SA material and the guided light in fiber, making it highly effective for nonlinear optical interactions. Tapered fiber is typically prepared by a heat and pulling system, where flame is used to soften an optical fiber, which is further stretched to achieve a microfiber with low optical losses. The schematic diagram of the tapered fiber is illustrated in Figure 6. The reduced diameter of the fiber, up to 30 μm [139] due to tapering, allows the extension of the evanescent field beyond the core to interact with the surrounding GO/rGO SA material. This configuration allows maximum interaction between the light traveling through the fiber and the GO/rGO SA material, enhancing the nonlinear optical character of SA, facilitating efficient pulse generation in SA. The parameters such as waist diameter and fiber length ensure the maintenance of balance between optical losses and the evanescent field interaction with GO/rGO SA material, occurring evenly in all directions. The evanescent field is the portion of the optical fiber that extends beyond the fiber core and maintains its interaction with the SA material to modify its nonlinear optical properties. Various means are used to deposit GO/rGO SA upon tapered fiber, a few of which are mentioned below.
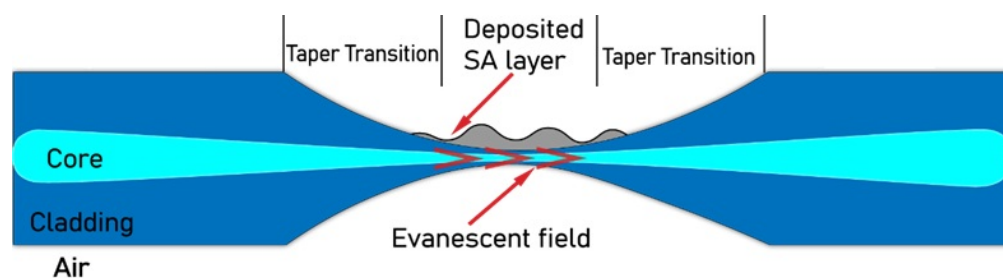

Figure 6. Schematics of the tapered optical fiber.

Dip coating is widely used to deposit oxide SA upon tapered fiber by dipping microfiber into the solution and then drying it to achieve the coating. Ng et al. investigated the deposition of reduced graphene oxide (rGO) upon the tapered fiber by dip coating [109]. The tapered fiber with a 10 μm waist was dipped for 20 s and then dried for 24 h to achieve a uniform coating upon the tapered region [109]. Moreover, the process is performed to stabilize the coating and maintain the intactness of the system for reliable performance in laser operations. This method ensures the uniform deposition of rGO SA upon the tapered region and ensures an improved light–matter interaction, critical for achieving consistent nonlinear optical properties across the SA layer. However, the efficiency of this process is limited due to the slow speed and blockage ability, which would impact the performance of the SA [140].

Another method, involving use of the micropipette, is to precisely place the GO/rGO SA material solution upon the tapered fiber. Jaddoa et al. reported the use of a micropipette to apply a small drop, i.e., 0.5 μL, of GO solution upon the waist of the tapered fiber [139]. The usage of a micropipette offers precise application of the GO solution to ensure the fabrication of GO SA at the interaction point of the strongest evanescent field. The direct deposition of the GO solution on the waist further facilitates the interaction between the evanescent field and the surrounding material, enhancing GO SA's nonlinear optical character. It ensures the minimization of unnecessary material use and ensures the placement of a thin GO layer around the fiber waist. However, the precision in placing a small quantity of GO SA enhances the risk of contamination or uneven application, causing the degradation of the SA's performance.

Tapered fibers hold a strong place in the domain of integration of SA into EDFLs due to the evanescent field interaction. They facilitate the generation of short pulses in EDFLs by enhancing the saturation efficiency at lower power levels [141]. However, the synthesis

of the tapered fiber requires precision, as poor control over the tapering process may lead to uneven tapering, resulting in excess loss or damage. High-power conditions may lead to mechanical fragility in the tapered region, which can reduce the efficiency and stability of the EDFL system. Moreover, the increase in insertion loss is observed after coating the SA material upon the tapered fiber. These losses are expected due to light absorption by GO/rGO SA materials. However, they can be overcome by significant improvements in the nonlinear properties of the oxide SA, which are crucial for stable pulse operation.

3.3. D-Shaped Fibers as SAs

D-shaped fiber is fabricated by partially removing the cladding layer from the optical fiber, paving the way for an enhanced interaction between the core's optical mode and external materials, such as GO/rGO SAs [142]. The schematic of the D-shaped fiber is depicted in Figure 7. It offers an enhanced light–matter interaction due to the direct contact of the SA with the guided light in the exposed core, making it ideal for SA integration. The strong interaction plays a key role in modulating the nonlinear optical properties of GO/rGO SA material for efficient pulse operation. The interaction is further enhanced by maintaining the distance between the fiber core and the flat D-shaped surface to an optimized value, i.e., 2 μm [143]. The thin residual cladding of the D-shaped fiber up to 5 μm [122] and interaction length of 10 mm [143] ensure the direct interaction of the GO/rGO SA material with light traveling in the core. Various methods are employed to deposit oxide SA upon the D-shaped fiber, some of which are discussed below.
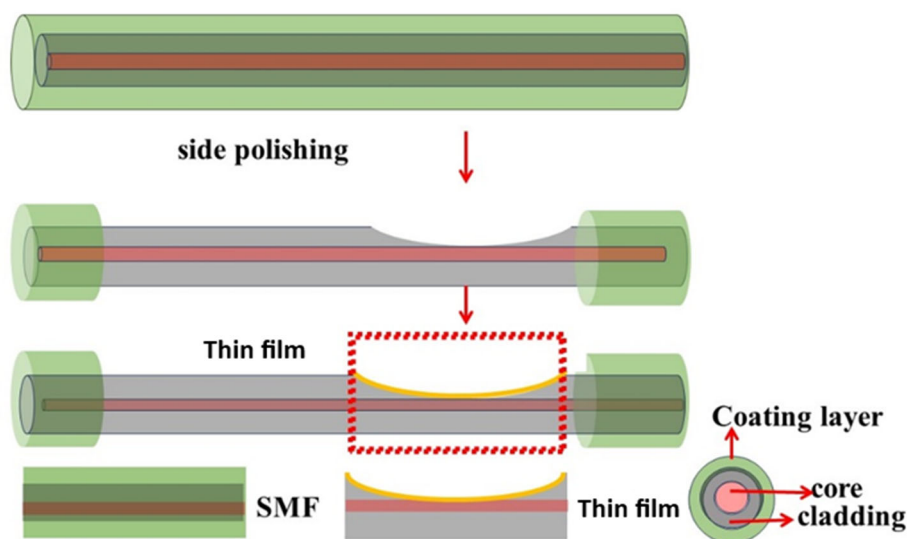

Figure 7. Schematics of the D-shaped optical fiber.

Drop-casting is a well-known technique used to prepare uniform thin films by dispersing the SA solution upon the polymer matrix, i.e., D-shaped fiber. Ahmed et al. reported the drop-casting of 0.2 mL of rGO solution upon the polished region of the D-shaped fiber, followed by drying for a suitable time of up to 2 h [144]. By controlling the solvent concentration and evaporation rate, the agglomeration is avoided, and an even rGO layer is obtained that acts as cladding for the polished fiber. This technique offers valuable advantages of an improved interaction area along with polarization insensitivity [145]. However, enhanced sensitivity toward the evaporation rate can cause a loss of control over the film thickness, which limits its use at a large scale [146].

Lee et al. reported the spraying of graphene oxide SA upon the polished upper cladding of the D-shaped fiber to create a polarization-sensitive SA [122]. The evanescent field interaction takes place among the GO layer and the fiber core, which creates strong polarization-dependent effects. It modulates the D-shaped fiber to act as an SA as well as a polarizer to facilitate stable pulse generation in a fiber laser. Its high polarization-dependent

loss, i.e., 20.73 dB, further leverages in polarization-sensitive applications, including Q-switching and mode-locking, which requires stable and high-contrast pulse generation.

Hence, the unique design of the D-shaped fiber raises an unparalleled evanescent field interaction that enhances its suitability for advanced fiber laser systems for stable pulse operation at low power levels. However, its fabrication is far more complex and needs technical expertise compared to other traditional fiber structures, making it less commonly used in EDFLs than other optical components, such as direct deposition of SAs on fiber ferrules and tapered fibers.

In conclusion, every method for the integration of SAs into the EDFL cavity brings its unique advantages and challenges. Fiber ferrules offer low-loss solutions along with compactness, while tapered and D-shaped fibers enhance the light–matter interaction via evanescent field exposure. Ultimately, the choice of method depends upon the specific properties of the material being used as well as the desired laser characteristics, such as the pulse duration, modulation depth, and power handling capability.

4. Performance of Q-Switched and Mode-Locked Erbium-Doped Fiber Lasers Based on GO/rGO Saturable Absorbers

GO/rGO nanomaterials are well-known materials used to implement inside the laser cavity to act as SAs in the form of a thin film that generates efficient ultrashort and ultrafast laser pulses. Q-switching is a distinct technique that rises from the nonlinear optical properties of SA materials, leading toward energy buildup within the laser cavity below a particular threshold pump power. However, when this threshold power and required gain are achieved inside the laser cavity, then Q-switching initiates, and the laser operates in pulsed mode. Q-switching is important because it allows EDFLs to achieve high peak powers, making them suitable for applications requiring short, intense bursts of light. In an EDFL setup incorporating GO and rGO as SAs, the laser cavity typically follows a ring configuration, as depicted in Figure 8. The key components include a pump laser, EDF, wavelength division multiplexer (WDM), isolator, and coupler, with the SA integrated to modulate the laser pulses. The diode pump laser emitting at 980 nm or 1480 nm is normally employed to excite the EDF using a WDM. GO/rGO is incorporated as a thin film on a fiber ferrule and then incorporated within the ring cavity via FC/PC connectors. GO/rGO act as an SA, exploiting their nonlinear optical properties to initiate a passive Q-switching or mode-locking mechanism within the cavity. When low-intensity light passes through, GO/rGO absorbs the light, but at higher intensities, it saturates and allows the light to pass, creating the pulses. An optical isolator (ISO) ensures unidirectional propagation of optical light within the cavity that stops unwanted feedback. Additionally, the output coupler extracts a portion of the laser output and divides it into required percentages. Furthermore, the data are analyzed using an optical spectrum analyzer (OSA), electric spectrum analyzer (ESA), and oscilloscope.

Mode-locking is an advanced form of Q-switching: the phases of different longitudinal modes of the laser synchronize, forcing them to interfere constructively at regular intervals, helping the formation of a train of short pulses. Passive mode-locking, a type of mode-locking mechanism, in an EDFL can be achieved normally by incorporating additional SMF into the laser cavity. In this technique, SMF is used to tailor the dispersion and nonlinear effects in the cavity, which plays a crucial role in generating ultrashort pulses through mode-locking. The additional SMF serves in dispersion management inside the cavity. The fiber introduces a certain amount of group velocity dispersion (GVD) and nonlinear effects, such as self-phase modulation (SPM), which is crucial for soliton formation and is a common mode-locking mechanism in fiber lasers. In passive mode-locking, an SA (such as graphene or SESAM) is often used alongside the SMF. The SA provides intensity-dependent transmission, allowing higher-intensity light to pass while absorbing lower-intensity light, effectively shortening the pulse duration. The schematics of a mode-locked EDFL is illustrated in Figure 9.
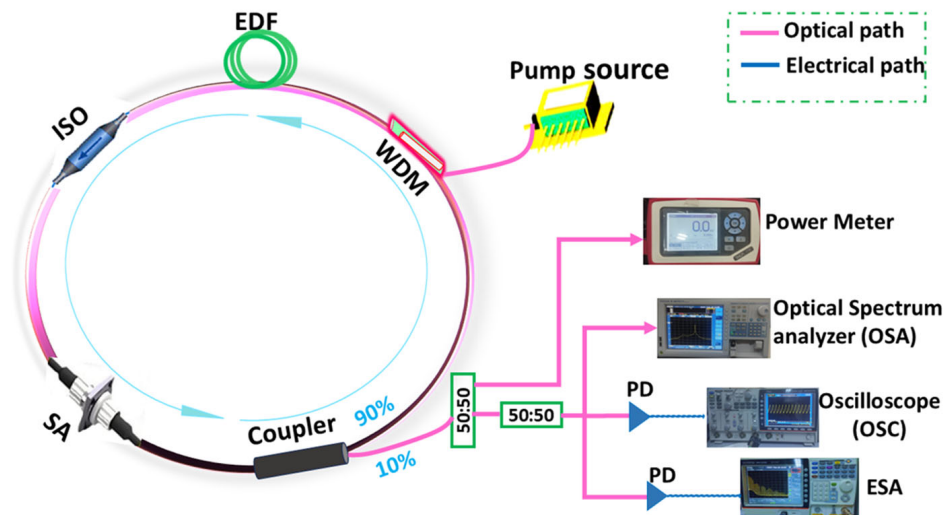
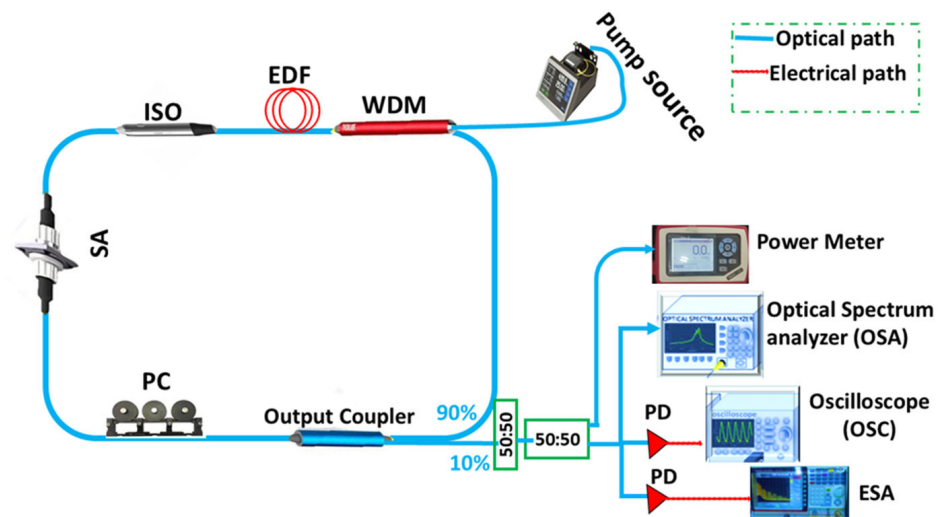**Figure 8.** Schematic of the experimental setup of a Q-switched EDFL.

Figure 9. Schematic of the experimental setup of a mode-locked EDFL.

In the following, we have summarized the performance of EDFL-based GO/rGO SAs. In the literature, for Q-switched EDFLs subject to GO SAs, the shortest pulse width of 1.2 µs was reported by Tiu et al. [121]. The achievement of the shortest pulse width can be attributed to the enhanced saturable absorption efficiency of GO, which is directly influenced by the structural defects, as discussed in Section 2.3. The proposed EDFL system yielded repetition rates of 16.3 kHz, and a pulse energy of 1.57 nJ. Additionally, the multi-wavelength operation of EDFL was acquired by employing a nonlinear polarization effect [121]. Su et al. reported that Q-switched EDFLs with rGO SAs generated pulses with the shortest pulse duration of 1.83 µs and attained the maximum repetition rate of 94.88 kHz [126]. The oxygen-containing groups of GO were thermally reduced to synthesize a uniform rGO sample, which gained an enhanced modulation depth of 5.8% and directly influenced the third-order nonlinearity of rGO SAs, i.e., saturable absorption, cross-phase modulation, Kerr effect, etc., resulting in a significant improvement in the repetition rate and pulse width of pulses [126]. On the other hand, Gerosa et al. reported a comprehensive analysis of GO and rGO SAs, mode-locked EDFL, and the shortest pulse width of 350 fs, with corresponding highest repetition rates of 48 MHz [147]. These results can be attributed to the unique approach of coating microcapillaries of photonic crystal fiber with GO and rGO samples. This approach of inserting rGO SA within the EDFL cavity reduced insertion and splicing losses, leading to the generation of pulses with improved stability

and pulse parameters, as mentioned above. Mansoor et al. reported the Q-switched EDFL with a maximum repetition rate of 123.5 kHz with a GO SA due to enhanced saturation of the SA proportional to the increase in pump power [148]. The proposed system emitted at 1558.75 nm, with 1.68 nJ of corresponding pulse energy and a 2.3 μs pulse duration [148]. On the other hand, Chen et al. reported the rGO SA with a uniform structure and optimal modulation depth of 5.5% due to strong thermal reduction, resulting in a high nonlinear saturation intensity [125]. It contributed to yielding a maximum repetition rate of 12.66 MHz, achieved by the mode-locked EDFL attaining rGO SA [125]. For Q-switched EDFLs with the GO SA, Tiu et al. reported a maximum average output power of 23.5 mW resulting from an enhanced nonlinear optical character, as discussed above [121]. For mode-locked EDFLs, Harun et al. investigated the maximum average output power of 33.7 mW achieved by the GO SA, resulting from improved third-order nonlinearity, reduced saturation losses, and a high damage threshold due to a four-layer GO paper [149]. Similarly, for Q-switched EDFLs with the rGO SA, Su et al. reported a maximum average output power of 14.65 mW [126]. On the other hand, Chen et al. investigated the maximum average output power of 18.22 mW for mode-locked EDFLs attaining rGO SAs [125]. The maximum SNR of 60 dB was reported by Mat et al. for Q-switched EDFLs with GO SAs, indicating the enhanced stability of the proposed system [113]. On the other hand, Ahmad et al. reported the maximum SNR values of 55.03 dB for Q-switched EDFLs with rGO SAs coated on arc-shaped fiber [107]. The concerned rGO SA showed an enhanced modulation depth of 23%, which readily enhanced its saturable absorption ability, leading to the generation of stable pulses with SNR values. Mode-locked EDFLs with GO SAs also achieved stable pulses with a maximum SNR value of 74 dB, as reported by Chen et al. [150]. He et al. reported the interaction of rGO with the evanescent field of microfiber, which stimulated the saturable absorption of rGO SAs, resulting in the generation of stable pulses with a maximum SNR of 70 dB for mode-locked EDFLs [151]. The maximum Q-switching range of 78.4 to 379.3 mW for Q-switched EDFLs with GO SAs was reported by Zhao et al., depicting the stability and high damage threshold of the SAs [152]. Su et al. investigated the maximum Q-switching range up to 90 to 289 mW with the rGO SA [126]. For mode-locked EDFLs with GO SAs, the maximum threshold range of 139 to 500 mW was reported by Xu et al. [153]. Meanwhile, Chen et al. investigated the maximum threshold power range of 273 to 563.07 mW for mode-locked EDFLs [125].

A summary of important parameters of pulses generated by Q-switched and mode-locked EDFLs utilizing GO/rGO SAs is presented in Table 1. The crucial parameters of EDFLs that determine their efficiency include the modulation depth of GO/rGO SAs, pulse duration, repetition rates, average output power, pulse energy, peak power, SNR, and Q-switching range, characterizing the performance of the proposed laser system.

Despite the generation of ultrashort optical pulses, the fabrication of ideal GO and rGO SAs for EDFLs presents several key challenges. First, achieving uniformity and controllability in the oxidation and reduction processes is critical, as these steps directly affect the GO/rGO SAs' optical and electronic properties. An insufficiently controlled oxidation process can lead to a non-uniform distribution of oxygen functional groups, affecting the saturable absorption behavior. Moreover, over-reduction of GO can result in the loss of oxygenated sites, compromising the tunability of the material's bandgap and saturable absorption parameters. Another challenge lies in the dispersibility and integration of GO and rGO into the fiber laser system. The tendency of graphene derivatives to aggregate can lead to optical losses and inefficient interaction with the laser beam. Additionally, ensuring the long-term stability of the SA is crucial, as GO and rGO can degrade under prolonged laser exposure or due to environmental factors, such as humidity or temperature changes.

Table 1. Summary of important parameters of pulses generated by Q-switched and mode-locked EDFLs utilizing GO/rGO SAs.

SA	Opr	MD (%)	PD (μs/ps)	RR (kHz/MHz)	P_{avg} (mW)	PP (mW/kW)	PE (nJ)	SNR (dB)	QS Range (mW)	Ref.
GO	QS	35	12	16	1.3	-	-	-	60–170	[154]
GO	QS	-	14.3	14.4	-	-	-	-	99–111.32	[117]
rGO	QS	7	2.0	85	2.2	13	26		10–85.0	[106]
GO	QS	24.1	2.9	65.27	0.99	-	15.17	45.13	200.5–225.1	[118]
GO	QS	-	4.73	51.81	0.128	0.52	2.47	52	26.32–71.65	[40]
GO	QS	-	5.67	81.7	8.93	-	109.3	-	16.88–72.85	[155]
GO	QS	3.7	7.8	17.8	2.3	15.4	128.1	42	105.2–193.6	[156]
GO	QS-ML	-	2.6	71.74	0.136	-	668.95	37	21.7–47.9	[119]
rGO	QS	5.8	1.83	94.88	14.65	-	154.34		90–280	[126]
rGO	QS	23	2.01	54.10	0.405	-	7.499	55.03	32.42–119.50	[107]
GO	QS	-	2.3	123.5	-	-	1.68	-	-	[148]
rGO	QS	3.2	3.53	-	2.27	-	48.19	-	50–170	[116]
GO	QS	-	3.6	39.1	1.32	-	33.8	38.8	26.4–79.0	[120]
GO	QS	-	5.57	61.77	0.003	-	0.054	-	39–96	[113]
GO	QS	-	2.28	53.45	0.042	-	0.78	38	56.17–105.98	[139]
GO	QS	-	1.2	16.3	23.5	-	1.57	-	39.6–46.8	[121]
GO	QS	-	2.48	22.5	0.788	-	40.69	-	33.7–59.5	[157]
GO	QS	-	7.7	27.2	0.11	-	4.3	31	65–118	[112]
GO	QS	-	3.90	57.0	0.17	-	81	-	10–70	[158]
GO	QS	8.6	2.12	8.96		-		-	162	[122]
rGO	QS	-	1.85	116	14.6	-	125	-	120–175	[115]
GO	QS	-	6.6	61	3.7	9.3	61.3	-	9–100	[159]
GO	QS	-	2.72	72.25	16.6	-	229.7	∼40	78.4–379.3	[152]
GO	ML	-	0.8	22	3.37	-	0.153	35.8	39.3–170.2	[133]
GO	ML	-	688,000	1.48	-	-	-	-	200	[117]
GO	ML	-	1.1	-	-	-	-	3	-	[160]
GO	ML	18.4	0.81	9.4	-	-	-	50.7	80	[161]
GO	ML	1.94	0.52	25.2	0.242	-	-	48.89	26.8	[114]
GO	ML	-	1.3	12.8	-	-	-	-	-	[162]
rGO	ML	3.9	0.57	5.68	6.75	-	1.19	59.5	40	[109]
GO	ML	24.1	0.8	22.0	33.7	-	1.53	35.8	39.3–170.2	[149]
GO	ML	-	0.35	48	-	-	-	-	-	[147]
rGO	ML	5.5	1380	12.66	18.22	-	1.44	50	273–563.07	[125]
GO	ML	-	1.18	16.5	-	-	-	58.3	76.6–280.5	[123]
rGO	ML	6.5	0.5	23.8	1.80	-	-	-	212	[131]
GO and rGO	ML	-	0.19	15.726 and 15.729	0.2	0.277	0.083	74	40	[105]
GO	ML	-	1.25	21.8	0.363	0.0113	0.015	-	70–175	[163]
GO	ML	1.96	0.9538	-	0.212	-	-	-	-	[130]
GO	ML	-	0.2	22.9						[129]
GO	ML	3.15	0.587	15.9	2.5	0.267	0.16	74	45–83	[150]
GO	ML	-	0.68	15.62	0.134	0.01185	0.0085	30	1.75–24.4	[164]
GO	ML	-	0.542	19.5	23.3	-	1.2	65	139–500	[153]
GO and rGO	ML	18 and 21	0.39	-	1.96 and 1.68	0.0864 and 0.0764	33.7 and 29.8	60	37 to 95 and 33 to 82	[128]
GO	ML	-	0.2	22.9	5.8	0.22	0.13	-	33–98	[165]
rGO	ML	5.75	26	7.47	1.2	-	-	70	35–166	[151]
GO	ML	-	0.9	17.5	-	-	1	-	-	[127]
rGO	ML	-	1.17	16.79	-	-	-	-	64.44–280.5	[144]

To address these challenges, precise control over chemical processes, such as Hummers' method for oxidation and subsequent thermal or chemical reduction, is essential. Optimizing the degree of oxidation and reduction allows for better tunability of the SAs' properties. Furthermore, functionalizing the GO or rGO with polymers or other stabilizers can improve dispersibility and prevent aggregation, ensuring uniform interactions with the laser light. Encapsulating the SA in a protective environment or integrating it into fiber-compatible composite materials can enhance its environmental and operational stability. Finally, advanced characterization techniques, such as Raman spectroscopy, X-ray photoelectron spectroscopy (XPS), and transmission electron microscopy (TEM), can help in fine-tuning the structural properties of GO and rGO to meet the specific requirements of EDFLs.

5. Conclusions

In conclusion, this review highlighted the significant advancements in the application of graphene oxide and reduced graphene oxide saturable absorbers for erbium-doped fiber lasers in both mode-locking and Q-switching regimes. The performance of these SAs has been extensively discussed, with a focus on key parameters, such as the pulse duration, repetition rate, average power, pulse energy, peak power, and signal-to-noise ratio. The comparative analysis showed that GO- and rGO-based SAs offer tunable optical properties that make them highly effective in generating ultrashort pulses and stable Q-switched operation, with excellent control over laser dynamics. However, the performance metrics are closely linked to the synthesis and fabrication techniques of GO and rGO thin films, as well as the methods used to incorporate them into the laser cavity. The various chemical and physical approaches for synthesizing these materials, including oxidation and reduction strategies, directly influence their saturable absorption characteristics, thereby impacting the laser output. Additionally, the integration methods—whether fiber end-face deposition, optical deposition, or film embedding—play a critical role in determining the stability and efficiency of the EDFL systems. Further advancements in fabrication techniques and material processing are necessary to optimize the performance of GO and rGO SAs, paving the way for more efficient and stable fiber laser systems in diverse applications.

References

1. Kumar, C.; Paul, C.P.; Das, M.; Bindra, K.S. Chapter 2—Fiber laser welding of Ti-6Al-4V alloy. In *Advanced Welding and Deforming*; Gupta, K., Davim, J.P., Eds.; Elsevier: Amsterdam, The Netherlands, 2021; pp. 23–66.
2. Sen, R.; Saha, M.; Das Chowdhury, S.; Shekhar, N.K.; Pal, D.; Ghosh, A.; Dhar, A.; Pal, A.; Pal, M. High Power Fiber Lasers: Fundamentals To Applications. *Sci. Cult.* **2015**, *81*, 319–326.
3. Shi, W.; Schulzgen, A.; Amezcua, R.; Zhu, X.; Alam, S.-U. Fiber lasers and their applications: Introduction. *J. Opt. Soc. Am. B* **2017**, *34*, FLA1. [CrossRef]
4. Churkin, D.V.; Sugavanam, S.; Vatnik, I.D.; Wang, Z.; Podivilov, E.V.; Babin, S.A.; Rao, Y.; Turitsyn, S.K. Recent advances in fundamentals and applications of random fiber lasers. *Adv. Opt. Photonics* **2015**, *7*, 516–569. [CrossRef]

5. Castillo-Guzman, A.; Anzueto-Sánchez, G.; Selvas, R.; Estudillo-Ayala, J.M.; Rojas-Laguna, R.; May-Arrioja, D.; Martinez-Rios, A. Erbium-doped tunable fiber laser. *Proc. SPIE* **2008**, *7062*, 70620Y. [CrossRef]

6. Kabir, M.; Hossain, M.; Amin, Z.; Ahsan, M.S. A theoretical investigation of erbium-doped fiber laser as a function of ion-clustering, temperature, pumping wavelength, and configuration. *Microw. Opt. Technol. Lett.* **2019**, *62*, 531–539. [CrossRef]

7. Bellemare, A. Continuous-wave silica-based erbium-doped fibre lasers. *Prog. Quantum Electron.* **2003**, *27*, 211–266. [CrossRef]

8. Hameed, H.; Asghar, H.; Liaqat, U.; Sohail, M.; Ahmed, R.; Umar, Z.A.; Baig, M.A. Fe-MOF as a novel saturable-absorber for pulse operation in erbium-doped fiber lasers. *Opt. Fiber Technol.* **2024**, *84*, 103771. [CrossRef]

9. Asghar, H.; Ahmed, R.; Sohail, M.; Umar, Z.A.; Baig, M.A. Q-switched pulse operation in erbium-doped fiber laser subject to CdS nanoparticles-based saturable absorber deposit directly on the fiber ferrule. *Opt. Mater.* **2022**, *134*, 113109. [CrossRef]

10. Asghar, M.; Ahmed, R.; Aslam Baig, M.; Asghar, H. On the performance of a Q-switched erbium-doped fiber laser based on a cadmium-sulfide (CdS) thin-film saturable absorber. *Opt. Contin.* **2024**, *3*, 1528–1539. [CrossRef]

11. Subramaniam, T. Erbium Doped Fiber Lasers for Long Distance Communication Using Network of Fiber Optics. *Am. J. Opt. Photonics* **2015**, *3*, 34–37. [CrossRef]

12. Khalid, U.S.; Asghar, H.; Hameed, H.; Sohail, M.; Khalil, A.; Ahmed, R.; Umar, Z.A.; Iqbal, J.; Baig, M.A. Q-switched pulse operation in erbium-doped fiber laser subject to zirconia (ZrO_2) nanoparticles-based saturable absorber. *Heliyon* **2024**, *10*, e24478. [CrossRef]

13. Yusoff, R.a.A.M.; Jafry, A.A.A.; Kasim, N.; Zulkipli, N.F.; Yasin, M.; Harun, S.W. Generation of Q-switched and mode-locked pulses using neodymium oxide as saturable absorber. *Results Opt.* **2020**, *1*, 100032. [CrossRef]

14. Ahmad, A.D.; Salam, S.; Mokhtar, N.; Arof, H.; Apsari, R.; Hamida, B.A.; Harun, S.W. Q-switched pulse generation in L-band region with polyacrylonitrile saturable absorber. *Phys. Scr.* **2024**, *99*, 065562. [CrossRef]

15. Keller, U. *Q-Switching*; Springer International Publishing: Cham, Germany, 2022; pp. 373–418.

16. Demesh, M.; Marzahl, D.-T.; Yasukevich, A.s.; Kisel, V.; Huber, G.; Kuleshov, N.; Kränkel, C. Passively Q-switched Pr:YLF laser with a Co:MgAl2O4 saturable absorber. *Opt. Lett.* **2017**, *42*, 4687. [CrossRef] [PubMed]

17. Dong, J.; Deng, P.; Liu, Y.; Zhang, Y.; Xu, J.; Chen, W.; Xie, X. Passively Q-switched Yb:YAG laser with Cr4+:YAG as the saturable absorber. *Appl. Opt.* **2001**, *40*, 4303–4307. [CrossRef] [PubMed]

18. Kir'yanov, A.; Filippov, V.; Starodumov, A. Cw-pumped erbium-doped fiber laser passively Q switched with Co 2+:ZnSe crystal: Modeling and experimental study. *J. Opt. Soc. Am. B* **2002**, *19*, 353–359. [CrossRef]

19. Luo, H.; Yang, J.; Li, J.; Liu, Y. Widely tunable passively Q-switched Er 3+-doped ZrF 4 fiber laser in the range of 3.4–3.7 μm based on a Fe 2+: ZnSe crystal. *Photonics Res.* **2019**, *7*, 1106–1111. [CrossRef]

20. Tang, J.; Bai, Z.; Zhang, D.; Qi, Y.; Ding, J.; Wang, Y.; Lu, Z. Advances in All-Solid-State Passively Q-Switched Lasers Based on Cr4+:YAG Saturable Absorber. *Photonics* **2021**, *8*, 93. [CrossRef]

21. Yang, Z.; Zhang, Z.; Cong, Z.; Liu, P.; Zhao, Z.; Su, L.; Liu, Z. Continuous-wave and Fe2+:ZnSe passively Q-switched mid-infrared lasers based on 2at.% Er3+:CaF2 crystal. *Results Opt.* **2024**, *15*, 100650. [CrossRef]

22. Yuxin, L.; Haihe, L.; Lihuang, L.; Zhizhan, X. Active–passive mode-locking using Cr4+:YAG crystal as saturable absorber. *Opt. Laser Technol.* **2001**, *33*, 403–407. [CrossRef]

23. Dai, L.; Huang, Z.; Huang, Q.; Zhao, C.; Rozhin, A.; Sergeyev, S.; Araimi, M.A.; Mou, C. Carbon nanotube mode-locked fiber lasers: Recent progress and perspectives. *Nanophotonics* **2021**, *10*, 749–775. [CrossRef]

24. Dvoretskiy, D.A.; Sazonkin, S.G.; Orekhov, I.O.; Kudelin, I.S.; Denisov, L.K.; Karasik, V.E.; Agafonov, V.N.; Khabashesku, V.N.; Davydov, V.A. Femtosecond Er-Doped All-Fiber Laser with High-Density Well-Aligned Carbon-Nanotube-Based Thin-Film Saturable Absorber. *Nanomaterials* **2022**, *12*, 3864. [CrossRef] [PubMed]

25. Huang, L.; Zhang, Y.; Liu, X. Dynamics of carbon nanotube-based mode-locking fiber lasers. *Nanophotonics* **2020**, *9*, 2731–2761. [CrossRef]

26. Lu, B.; Zou, C.; Huang, Q.; Huang, Z.; AlAraimi, M.; Mou, C.; Luo, Z.; Rozhin, A. Wavelength-tunable bidirectional passively Q-switched Er-doped fiber laser incorporating a single-walled carbon nanotube and tunable bandpass filter. *Appl. Opt.* **2020**, *59*, 2709–2714. [CrossRef] [PubMed]

27. Lü, Y.; Wei, C.; Zhang, H.; Kang, Z.; Qin, G.; Liu, Y. Wideband tunable passively Q-switched fiber laser at 2.8 μm using a broadband carbon nanotube saturable absorber. *Photonics Res.* **2018**, *7*, 14–18. [CrossRef]

28. Nishizawa, N.; Seno, Y.; Sumimura, K.; Sakakibara, Y.; Itoga, E.; Kataura, H.; Itoh, K. All-polarization-maintaining Er-doped ultrashort-pulse fiber laser using carbon nanotube saturable absorber. *Opt. Express* **2008**, *16*, 9429–9435. [CrossRef] [PubMed]

29. Rifin, S.N.M.; Munajat, Y.; Razak, S.N.A.; Zulkifli, M.Z.; Ahmad, H. 68 MHz Fundamental Repetition Rates for Mode-Locked Erbium Doped Fiber Laser based Carbon Nanotube Saturable Absorber. *J. Phys. Conf. Ser.* **2020**, *1529*, 042003. [CrossRef]

30. Sohail, M.; Nawaz, A.; Alomar, M.; Khan, S.A.; Hussain, A.; Khan, N.Z.; Hayat, Q.; Ali, J.; Muhammad, Y.; Asghar, H.; et al. Carbon nanomaterials as nonlinear optical modulators for pulsed laser generation at near-infrared region. *Phys. B Condens. Matter* **2024**, *674*, 415519. [CrossRef]

31. Sohail, M.; Zhang, C.; Ahmed, R.; Asghar, H.; Ali Khan, S.; Zamin Khan, N.; Chen, T.; Baig, M.A.; Wang, Z. Carbon nanoparticles (CNPs) as a saturable absorber for a passively Q-switched erbium (Er3+) doped fiber laser. *Opt. Laser Technol.* **2023**, *160*, 109046. [CrossRef]

32. Ahmed, M.H.M.; Latiff, A.A.; Arof, H.; Harun, S.W. Ultrafast erbium-doped fiber laser mode-locked with a black phosphorus saturable absorber. *Laser Phys. Lett.* **2016**, *13*, 095104. [CrossRef]

33. Alghamdi, T.A.; Adwan, S.; Arof, H.; Harun, S.W. Application of black phosphorus for pulse generation in erbium-doped fiber laser. *Results Opt.* **2021**, *4*, 100091. [CrossRef]

34. Alghamdi, T.A.; Adwan, S.; Arof, H.; Harun, S.W. Q-switched triple-wavelength erbium-doped fiber laser with black phosphorus absorber. *Optik* **2024**, *311*, 171874. [CrossRef]

35. Hu, Y.; Jin, X.; Hu, G.; Zhang, M.; Wu, Q.; Zheng, Z.; Hasan, T. Hybrid mode-locked erbium-doped fiber laser with black phosphorus saturable absorber. In Proceedings of the 2018 Conference on Lasers and Electro-Optics (CLEO), San Jose, CA, USA, 13–18 May 2018; pp. 1–2.

36. Li, J.; Luo, H.; Zhai, B.; Lu, R.; Guo, Z.; Zhang, H.; Liu, Y. Black phosphorus: A two-dimension saturable absorption material for mid-infrared Q-switched and mode-locked fiber lasers. *Sci. Rep.* **2016**, *6*, 30361. [CrossRef]

37. Liu, X.; Gao, Q.; Zheng, Y.; Mao, D.; Zhao, J. Recent progress of pulsed fiber lasers based on transition-metal dichalcogenides and black phosphorus saturable absorbers. *Nanophotonics* **2020**, *9*, 2215–2231. [CrossRef]

38. Qin, Z.; Xie, G.; Zhao, C.; Yuan, P.; Wen, S.; Qian, L. Black phosphorus as saturable absorber for the Q-switched Er:ZBLAN fiber laser at 2.8 μm. *Opt. Express* **2015**, *23*, 24713–24718. [CrossRef]

39. Fu, S.; Chen, C.; Ge, Z.; Zhou, B. Passive Q-switched erbium-doped fiber laser based on graphene saturable absorber. In Proceedings of the International Symposium on Photonics and Optoelectronics (SOPO 2014), Suzhou, China, 22–24 August 2014; Volume 9233.

40. Huda, C.; Yasin, M.; Zaidan, A.; Harun, S.W.; Jafry, A.A.; Rosol, A. Passively Q-switched erbium-doped fiber laser with graphene oxide film as saturable absorber. *J. Phys. Conf. Ser.* **2021**, *1869*, 012158. [CrossRef]

41. Ismail, M.A.; Ahmad, F.; Harun, S.W.; Arof, H.; Ahmad, H. A Q-switched erbium-doped fiber laser with a graphene saturable absorber. *Laser Phys. Lett.* **2013**, *10*, 025102. [CrossRef]

42. Jasni, N.A.H.; Zuikafly, S.N.F.; Ahmad, F.; Abdullah, M.; Nawawi, W.M.F.W.; Yahaya, H. Graphene-Based Saturable Absorber for Passive Q-Switching Erbium Doped Fiber Laser. In Proceedings of the 2020 IEEE International Conference on Semiconductor Electronics (ICSE), Kuala Lumpur, Malaysia, 28–29 July 2020; pp. 124–127.

43. Rosdin, R.Z.R.R.; Ahmad, F.; Ali, N.M.; Harun, S.W.; Arof, H. Q-switched Er-doped fiber laser with low pumping threshold using graphene saturable absorber. *Chin. Opt. Lett.* **2014**, *12*, 091404. [CrossRef]

44. Wang, Z.T.; Chen, Y.; Zhao, C.J.; Zhang, H.; Wen, S.C. Switchable Dual-Wavelength Synchronously Q-Switched Erbium-Doped Fiber Laser Based on Graphene Saturable Absorber. *IEEE Photonics J.* **2012**, *4*, 869–876. [CrossRef]

45. Yang, X.F.; Wang, Y.; Huang, H.T.; Shen, D.Y.; Tang, D.Y.; Zhu, H.Y.; Xu, X.D.; Zhou, D.H.; Xu, J. A passively Q-switched Er:LuYAG laser with a graphene saturable absorber. *Laser Phys. Lett.* **2013**, *10*, 105810. [CrossRef]

46. Guo, Q.; Pan, J.; Li, D.; Shen, Y.; Han, X.; Gao, J.; Man, B.; Zhang, H.; Jiang, S. Versatile Mode-Locked Operations in an Er-Doped Fiber Laser with a Film-Type Indium Tin Oxide Saturable Absorber. *Nanomaterials* **2019**, *9*, 701. [CrossRef] [PubMed]

47. Guo, Q.; Si, H.; Lu, Z.; Han, X.; Man, B.; Feng, D.; Zhang, H.; Jiang, S. Passively mode-locked dual-wavelength Er-doped fiber laser based on antimony tin oxide as saturable absorber. *Laser Phys.* **2019**, *29*, 045801. [CrossRef]

48. Li, L.; Lv, R.; Chen, Z.; Wang, J.; Liu, S.; Ren, W.; Wang, Y. Mode-Locked Er-Doped Fiber Laser by Using MoS2/SiO2 Saturable Absorber. *Nanoscale Res. Lett.* **2019**, *14*, 59. [CrossRef] [PubMed]

49. Nady, A.; Ahmed, M.H.M.; Latiff, A.A.; Numan, A.; Raymond Ooi, C.H.; Harun, S.W. Nickel oxide nanoparticles as a saturable absorber for an all-fiber passively Q-switched erbium-doped fiber laser. *Laser Phys.* **2017**, *27*, 065105. [CrossRef]

50. Nady, A.; Latiff, A.A.; Numan, A.; Raymond Ooi, C.H.; Harun, S.W. Theoretical and experimental studies on a Q-switching operation in an erbium-doped fiber laser using vanadium oxide as saturable absorber. *Laser Phys.* **2018**, *28*, 085106. [CrossRef]

51. Nady, A.; Salhi, M.; Harun, S.W. Passively Q-switched erbium-doped fiber laser utilizing tungsten oxide as a saturable absorber. *Appl. Opt.* **2019**, *58*, 9768–9772. [CrossRef] [PubMed]

52. Zhang, M.; Hu, G.; Hu, G.; Howe, R.C.T.; Chen, L.; Zheng, Z.; Hasan, T. Yb- and Er-doped fiber laser Q-switched with an optically uniform, broadband WS2 saturable absorber. *Sci. Rep.* **2015**, *5*, 17482. [CrossRef]

53. Ding, G.; Zhang, Y.; Wang, L.; Zhang, Y.; Huang, J.; Liu, K.; Gu, Y.; Nie, Z.; Liu, G. Organic frame metal structure materials UIO-66 for picosecond ultrafast pulsed fiber lasers. *Laser Phys.* **2024**, *34*, 035101. [CrossRef]

54. Du, X.; Liu, H.; Li, S.; Ding, Z.; Liu, C.; Zhu, C.; Wang, P. Application of Pr-MOFs as saturable absorbers in ultrafast photonics. *J. Mater. Chem. C* **2024**, *12*, 5400–5410. [CrossRef]

55. Murad, A.; Mohd Yusoff, N.; Liew, J.Y.C.; Ng, E.K.; Alresheedi, M.T.; Abas, A.F.; Mahdi, M.A. Generation of noise-like pulse using nickel-based metal-organic framework saturable absorber. *Optik* **2023**, *290*, 171275. [CrossRef]

56. Murad, A.; Mohd Yusoff, N.; Liew, J.Y.C.; Yaacob, M.H.; Goh, C.S.; Mahdi, M.A. Nickel 1,3,5-benzene-tricarboxylic acid-metal organic framework polymer composite saturable absorber for femtosecond pulse generation. *Results Phys.* **2022**, *41*, 105881. [CrossRef]

57. Wang, P.; Zhu, C. Passively Q-Switched and Mode-Locked Fiber Laser Based on a Zeolitic Imidazolate Framework-67 Saturable Absorber. *Front. Phys.* **2022**, *10*, 926344. [CrossRef]

58. Xu, M.; Chu, H.; Pan, H.; Zhao, S.; Li, D. Highly stable passively Q-switched erbium-doped fiber laser with zeolitic imidazolate framework-67 saturable absorber. *Infrared Phys. Technol.* **2022**, *125*, 104274. [CrossRef]

59. Feng, J.; Li, X.; Feng, T.; Wang, Y.; Liu, J.; Zhang, H. Harmonic Mode-Locked Er-Doped Fiber Laser by Evanescent Field-Based MXene Ti3C2Tx (T = F, O, or OH) Saturable Absorber. *Ann. Phys.* **2020**, *532*, 1900437. [CrossRef]

60. Gao, B.; Li, Y.-Y.; Ma, C.-Y.; Shu, Y.-Q.; Wu, G.; Chen, B.-K.; Huo, J.-Y.; Han, Y.; Liu, L.; Zhang, Y. Ta4C3 MXene as a saturable absorber for femtosecond mode-locked fiber lasers. *J. Alloys Compd.* **2022**, *900*, 163529. [CrossRef]

61. Jhon, Y.I.; Koo, J.; Anasori, B.; Seo, M.; Lee, J.H.; Gogotsi, Y.; Jhon, Y.M. Metallic MXene Saturable Absorber for Femtosecond Mode-Locked Lasers. *Adv. Mater.* **2017**, *29*, 1702496. [CrossRef]

62. Lau, K.Y.; Liu, X.; Qiu, J. MXene Saturable Absorbers in Mode-Locked Fiber Laser. *Laser Photonics Rev.* **2022**, *16*, 2100709. [CrossRef]

63. Li, J.; Zhang, Z.; Du, L.; Miao, L.; Yi, J.; Huang, B.; Zou, Y.; Zhao, C.; Wen, S. Highly stable femtosecond pulse generation from a MXene Ti3C2Tx (T = F, O, or OH) mode-locked fiber laser. *Photonics Res.* **2019**, *7*, 260–264. [CrossRef]

64. Ma, C.; Huang, W.; Wang, Y.; Adams, J.; Wang, Z.; Liu, J.; Song, Y.; Ge, Y.; Guo, Z.; Hu, L.; et al. MXene saturable absorber enabled hybrid mode-locking technology: A new routine of advancing femtosecond fiber lasers performance. *Nanophotonics* **2020**, *9*, 2451–2458. [CrossRef]

65. Wu, Q.; Jin, X.; Chen, S.; Jiang, X.; Hu, Y.; Jiang, Q.; Wu, L.; Li, J.; Zheng, Z.; Zhang, M.; et al. MXene-based saturable absorber for femtosecond mode-locked fiber lasers. *Opt. Express* **2019**, *27*, 10159–10170. [CrossRef]

66. Ahmad, H.; Abdul Kahar, N.H.; Ramli, R.; Yusoff, N.; Reduan, S.A.; Ismail, M.F.; Lim, K.S.; Chong, W.Y.; Yasin, M. The performance of Ti2C MXene and Ti2AlC MAX Phase as saturable absorbers for passively mode-locked fiber laser. *Opt. Fiber Technol.* **2021**, *67*, 102683. [CrossRef]

67. Jafry, A.A.; Kasim, N.; Mohd Rusdi, M.; Rosol, A.; Yusoff, R.A.M.; Muhammad, A.R.; Nizamani, B.; Harun, S.W. MAX phase based saturable absorber for mode-locked erbium-doped fiber laser. *Opt. Laser Technol.* **2020**, *127*, 106186. [CrossRef]

68. Jafry, A.A.A.; Kasim, N.; Nizamani, B.; Muhammad, A.R.; Yusoff, R.a.A.M.; Harun, S.W.; Yupapin, P. MAX phase Ti3AlC2 embedded in PVA and deposited onto D-shaped fiber as a passive Q-switcher for erbium-doped fiber laser. *Optik* **2020**, *224*, 165682. [CrossRef]

69. Lee, J.; Kwon, S.; Lee, J.H. Ti2AlC-based saturable absorber for passive Q-switching of a fiber laser. *Opt. Mater. Express* **2019**, *9*, 2057–2066. [CrossRef]

70. Lee, J.; Kwon, S.-Y.; Lee, J.H. Harmonically mode-locked Er-doped fiber laser at 1.3 GHz using a V2AlC MAX phase nanoparticle-based saturable absorber. *Opt. Laser Technol.* **2022**, *145*, 107525. [CrossRef]

71. Sun, G.; Feng, M.; Zhang, K.; Wang, T.; Li, Y.; Han, D.; Li, Y.; Song, F. Q-Switched and Mode-Locked Er-doped fiber laser based on MAX phase Ti2AlC saturable absorber. *Results Phys.* **2021**, *26*, 104451. [CrossRef]

72. Zhao, B.; Zhang, H.-P.; Ma, R.-Z.; Farrell, G.; Li, Z.-R.; Wang, P.-F. Bimetallic solid solution MAX phase Ti2NbAlC2 as saturable absorber for passively Q-switched Er3+-doped fiber laser. *Laser Phys. Lett.* **2024**, *21*, 025101. [CrossRef]

73. Han, X. 2D MoTe2 film as a saturable absorber for a wavelength-tunable ultrafast fiber laser. *Appl. Opt.* **2019**, *58*, 8390–8395. [CrossRef] [PubMed]

74. Li, L.; Su, Y.; Wang, Y.; Wang, X.; Wang, Y.; Li, X.; Mao, D.; Si, J. Femtosecond Passively Er-Doped Mode-Locked Fiber Laser With WS2 Solution Saturable Absorber. *IEEE J. Sel. Top. Quantum Electron.* **2017**, *23*, 44–49. [CrossRef]

75. Liu, W.; Liu, M.; Lei, M.; Fang, S.; Wei, Z. Titanium Selenide Saturable Absorber Mirror for Passive Q-Switched Er-Doped Fiber Laser. *IEEE J. Sel. Top. Quantum Electron.* **2018**, *24*, 2759266. [CrossRef]

76. Omar, S.; Musa, B.; Jusoh, Z.; Ali, M.I.M.; Jafry, A.A.A.; Harun, S.W. Passively Q-switched Erbium-doped Fiber Laser using Tungsten Disulfide deposited D-shaped Fiber as Saturable Absorber. *IOP Conf. Ser. Mater. Sci. Eng.* **2020**, *854*, 012021. [CrossRef]

77. Shang, X.; Guo, L.; Zhang, H.; Li, D.; Yue, Q. Passive mode-locked Er-doped fiber laser pulse generation based on titanium disulfide saturable absorber. *Front. Inf. Technol. Electron. Eng.* **2021**, *22*, 756–766. [CrossRef]

78. Wei, B.-N.; Jiao, Z.-H.; Liu, W.-J. Ternary transition metal dichalcogenides for passively Q-switched Er-doped fiber laser applications. *Optik* **2021**, *248*, 168096. [CrossRef]

79. Woodward, R.I.; Howe, R.C.T.; Runcorn, T.H.; Hu, G.; Torrisi, F.; Kelleher, E.J.R.; Hasan, T. Wideband saturable absorption in few-layer molybdenum diselenide (MoSe2) for Q-switching Yb-, Er- and Tm-doped fiber lasers. *Opt. Express* **2015**, *23*, 20051–20061. [CrossRef] [PubMed]

80. Ahmed, H.; Asghar, H.; Hameed, H.; Ahmed, R.; Khalil, A.; Iqbal, J.; Alrebdi, T. Co/MoS2 nanocomposite for passive Q-switched pulse operation in erbium-doped fiber lasers. *Opt. Mater. Express* **2024**, *14*, 532935. [CrossRef]

81. Armas-Rivera, I.; Rodriguez-Morales, L.A.; Durán-Sánchez, M.; Avazpour, M.; Carrascosa, A.; Silvestre, E.; Kuzin, E.A.; Andrés, M.V.; Ibarra-Escamilla, B. Wide wavelength-tunable passive mode-locked Erbium-doped fiber laser with a SESAM. *Opt. Laser Technol.* **2021**, *134*, 106593. [CrossRef]

82. Fang, Z.; Zhang, C.; Liu, J.; Chen, Y.; Fan, D. 3.46 μm Q-switched Er3+:ZBLAN fiber laser based on a semiconductor saturable absorber mirror. *Opt. Laser Technol.* **2021**, *141*, 107131. [CrossRef]

83. Gao, X.; Zhao, Z.; Cong, Z.; Gao, G.; Zhang, A.; Guo, H.; Yao, G.; Liu, Z. Stable 5-GHz fundamental repetition rate passively SESAM mode-locked Er-doped silica fiber lasers. *Opt. Express* **2021**, *29*, 9021–9029. [CrossRef] [PubMed]

84. Ma, X.; Zhang, K.; Li, C.; Chen, K.; Zhou, Y.; Zhang, W.; Fang, W.; Chen, X.; Huang, S.; Yu, R.; et al. Decaying dynamics of harmonic mode-locking in a SESAM-based mode-locked fiber laser. *Opt. Express* **2023**, *31*, 36350–36358. [CrossRef]

85. Wang, S.; Tu, C.; Jamali Mahabadi, S.E.; Droste, S.; Sinclair, L.C.; Coddington, I.; Newbury, N.R.; Carruthers, T.F.; Menyuk, C.R. Obtaining more energetic modelocked pulses from a SESAM-based fiber laser. *Opt. Express* **2020**, *28*, 20345–20361. [CrossRef] [PubMed]

86. Yu, Z.; Ou, S.; Guo, L.; Zhang, Q.; Sui, Q.; Chen, Y.; Zhang, N.; Liu, H.; Shum, P.P. 109 fs, 553 MHz pulses from a polarization-maintaining Yb-doped ring fiber laser with SESAM mode-locking. *Opt. Commun.* **2022**, *522*, 128520. [CrossRef]
87. Zhang, Y.; Qi, Y.; Huo, X.; Chen, B.; Bai, Z.; Yang, X.; Ding, J.; Wang, Y.; Lu, Z. Study of the influence of SESAM parameters on the evolution of mode-locked pulses at different repetition rates. *Appl. Phys. B* **2021**, *127*, 119. [CrossRef]
88. Wang, M.; Zhang, F.; Wang, Z.; Xu, X. Liquid-Phase Exfoliated Silicon Nanosheets: Saturable Absorber for Solid-State Lasers. *Materials* **2019**, *12*, 201. [CrossRef] [PubMed]
89. Mohammed, D.Z.; Al-Janabi, A.H. Passively Q-switched erbium doped fiber laser based on double walled carbon nanotubes-polyvinyl alcohol saturable absorber. *Laser Phys.* **2016**, *26*, 115108. [CrossRef]
90. Kang, D.; Sarkar, S.; Kim, S. Highly Damage-Resistant Thin Film Saturable Absorber Based on Mechanically Functionalized SWCNTs. *Nanoscale Res. Lett.* **2022**, *17*, 11. [CrossRef] [PubMed]
91. Peng, X.; Yan, Y. Graphene saturable absorbers applications in fiber lasers. *J. Eur. Opt. Soc. Rapid Publ.* **2021**, *17*, 16. [CrossRef]
92. Shakaty, A.; Hmood, J.K.; Mhdi, B.R. Graphene-based Saturable Absorber for Pulsed Fiber Laser Generation. *J. Phys. Conf. Ser.* **2021**, *1795*, 012048. [CrossRef]
93. Li, D.; Yadav, A.; Zhou, H.; Roy, K.; Thanasekaran, P.; Lee, C. Advances and Applications of Metal-Organic Frameworks (MOFs) in Emerging Technologies: A Comprehensive Review. *Glob. Chall.* **2024**, *8*, 2300244. [CrossRef] [PubMed]
94. Lau, K.Y.; Hou, D. Recent research and advances of material-based saturable absorber in mode-locked fiber laser. *Opt. Laser Technol.* **2021**, *137*, 106826. [CrossRef]
95. Dahlqvist, M.; Barsoum, M.W.; Rosen, J. MAX phases—Past, present, and future. *Mater. Today* **2024**, *72*, 1–24. [CrossRef]
96. Lau, K.Y. Recent advances of MXene saturable absorber for near-infrared mode-locked fiber laser. *arXiv* **2021**, arXiv:2109.11.
97. Asghar, H.; Ahmed, R.; Umar, Z. A novel technique for the fabrication of a saturable absorber for fiber lasers: Pulsed laser deposition. *Laser Phys. Lett.* **2022**, *19*, 075106. [CrossRef]
98. Zhang, Y.; Lu, D.; Yu, H.; Zhang, H. Low-Dimensional Saturable Absorbers in the Visible Spectral Region. *Adv. Opt. Mater.* **2019**, *7*, 1800886. [CrossRef]
99. Asghar, H.; Ahmed, R.; Ajmal, R.; Umar, Z.A.; McInerney, J.G.; Baig, M.A. Ameliorating the stability of erbium-doped fiber laser using saturable absorber fabricated by the pulsed laser deposition technique. *Sci. Rep.* **2022**, *12*, 20267. [CrossRef] [PubMed]
100. Wu, H.; Wang, G.; Wang, X.; Xu, Y.; Shi, L.; Zhang, H.; Jin, L.; Ma, X.; Zou, Y.; Xu, L. Stable passively Q-switched erbium-doped fiber laser based on CuCrO2 nanoparticles saturable absorber. *Opt. Commun.* **2020**, *475*, 126222. [CrossRef]
101. Hussain, S.S.; Bibi, S.; Asghar, H.; Baig, M.A.; Ahmed, R. Comparative study of mesh powder and thin film of yttrium oxide (Y2O3) as saturable absorber. *Phys. B Condens. Matter* **2024**, *677*, 415739. [CrossRef]
102. Ajmal, R.; Bibi, S.; Ahmed, R.; Sohail, M.; Asghar, H.; Umar, Z.A.; Shahzad, N.; Baig, M.A. The role of saturable absorbers thickness in the Q-switching of the erbium-doped fiber laser. *Laser Phys. Lett.* **2023**, *20*, 035101. [CrossRef]
103. Asghar, H.; Khalid, U.; Sohail, M.; Alrebdi, T.; Umar, Z.; Alshehri, A.; Ahmed, R. Passively Q-Switched Er-Doped Fiber Laser Based on Bentonite Clay (Al2H2O6Si) Saturable Absorber. *Micromachines* **2024**, *15*, 267. [CrossRef] [PubMed]
104. Pan, H.; Chu, H.; Pan, Z.; Li, Y.; Zhao, S.; Li, D. Nonlinear optical properties of carboxyl-functionalized graphene oxide for dissipative soliton resonance pulse generation. *J. Mater.* **2023**, *9*, 642–650. [CrossRef]
105. Steinberg, D.; Gerosa, R.; Pellicer, F.; Zapata, J.; Domingues, S.; Souza, E.; Saito, L. Graphene oxide and reduced graphene oxide as saturable absorbers onto D-shaped fibers for sub 200-fs EDFL mode-locking. *Opt. Mater. Express* **2017**, *8*, 144. [CrossRef]
106. Yap, Y.; Chong, W.; Razgaleh, S.; Huang, N.; Ong, C.; Ahmad, H. Performance of Q-switched fiber laser using optically deposited reduced graphene oxide as saturable absorber. *Fiber Integr. Opt.* **2022**, *41*, 26–40. [CrossRef]
107. Ahmad, H.; Tajdidzadeh, M.; Reduan, S.A. Passively Q-switched erbium-doped fiber laser using coated reduced graphene oxide on arc-shaped single mode optical fiber as a saturable absorber. *Laser Phys.* **2018**, *28*, 085101. [CrossRef]
108. Sabran, M.; Ismail, M.; Azooz, S.; Ahmad, H.; Zulkifli, A.; Harun, S.W. Q-switching and mode-locking pulse generation with graphene oxide paper-based saturable absorber. *J. Eng.* **2015**, *2015*, 208–214.
109. Ng, E.K.; Lau, K.Y.; Lee, H.K.; Yusoff, N.M.; Sarmani, A.R.; Omar, M.F.; Mahdi, M.A. L-band femtosecond fiber laser based on a reduced graphene oxide polymer composite saturable absorber. *Opt. Mater. Express* **2021**, *11*, 59–72. [CrossRef]
110. Stankovich, S.; Dikin, D.A.; Dommett, G.H.B.; Kohlhaas, K.M.; Zimney, E.J.; Stach, E.A.; Piner, R.D.; Nguyen, S.T.; Ruoff, R.S. Graphene-based composite materials. *Nature* **2006**, *442*, 282–286. [CrossRef] [PubMed]
111. Lee, C.; Wei, X.; Kysar, J.; Hone, J. Measurement of the Elastic Properties and Intrinsic Strength of Monolayer Graphene. *Science* **2008**, *321*, 385–388. [CrossRef] [PubMed]
112. Ahmad, H.; Zulkifli, A.Z.; Kiat, Y.Y.; Harun, S.W. Q-switched fibre laser using 21cm Bismuth-erbium doped fibre and graphene oxide as saturable absorber. *Opt. Commun.* **2014**, *310*, 53–57. [CrossRef]
113. Mat, F.C.; Yasin, M.; Latiff, A.A.; Harun, S.W. Graphene oxide film as passive Q-switcher in erbium-doped fiber laser cavity. *Photonics Lett. Pol.* **2017**, *9*, 100–102. [CrossRef]
114. Ismail, M.; Razak, M.; Harun, S.W.; Hashim, A.M. Reduction-controlled graphene oxide saturable absorbers and its effect on ultrashort Er-doped fibre laser. *IET Optoelectron.* **2021**, *15*, 61–68. [CrossRef]
115. Sobon, G.; Sotor, J.; Jagiełło, J.; Kozinski, R.; Librant, K.; Zdrojek, M.; Lipińska, L.; Abramski, K. Linearly polarized, Q-switched Er-doped fiber laser based on reduced graphene oxide saturable absorber. *Appl. Phys. Lett.* **2012**, *101*, 241106. [CrossRef]
116. Li, L.; Lv, R.-D.; Liu, S.-C.; Chen, Z.-D.; Wang, J.; Wang, Y.-G.; Ren, W. Using Reduced Graphene Oxide to Generate Q-Switched Pulses in Er-Doped Fiber Laser. *Chin. Phys. Lett.* **2018**, *35*, 114202. [CrossRef]

117. Monteiro, C.S.; Perez-Herrera, R.A.; Silva, S.O.; Frazão, O. Short Pulse Generation in Erbium-Doped Fiber Lasers Using Graphene Oxide as a Saturable Absorber. In *PHOTOPTICS*; Science and Technology Publications, Lda: Lisbon, Portugal, 2023.

118. Noor, S.; Ahmad, B.; Rosol, A.; Ahmad, H.; Apsari, R.; Harun, S.W. Dual-wavelength Q-switched erbium-doped fiber laser using an SMF-MMF-SMF structure and graphene oxide. *Optoelectron. Lett.* **2022**, *18*, 668–672. [CrossRef]

119. Allah, B.; Eltaif, T.; Omer, M.; Khan, S. Investigation of Q-switched and Mode-Locked Erbium-Doped Fiber Laser Using Graphene oxide-Saturable Absorber. In Proceedings of the 2019 IEEE 14th Malaysia International Conference on Communication (MICC), Selangor, Malaysia, 2–4 December 2019; pp. 48–53.

120. Ahmad, H.; Zulkifli, A.Z.; Thambiratnam, K. Tunable Q-switched erbium-doped fiber laser based on curved multimode fiber and graphene oxide saturable absorber. *Laser Phys.* **2017**, *27*, 055103. [CrossRef]

121. Tiu, Z.C.; Ahmad, F.; Tan, S.J.; Ahmad, H.; Harun, S.W. Multi-wavelength Q-switched Erbium-doped fiber laser with photonic crystal fiber and graphene—Polyethylene oxide saturable absorber. *Optik* **2015**, *126*, 1495–1498. [CrossRef]

122. Lee, J.; Koo, J.; Debnath, P.; Song, Y.W.; Lee, J.H. A Q-switched, mode-locked fiber laser using a graphene oxide-based polarization sensitive saturable absorber. *Laser Phys. Lett.* **2013**, *10*, 035103. [CrossRef]

123. Ahmad, H.; Soltani, S.; Thambiratnam, K.; Yasin, M. Highly stable mode-locked fiber laser with graphene oxide-coated side-polished D-shaped fiber saturable absorber. *Opt. Eng.* **2018**, *57*, 1. [CrossRef]

124. Saha, S.K. Sensitivity of the mode locking phenomenon to geometric imperfections during wrinkling of supported thin films. *Int. J. Solids Struct.* **2017**, *109*, 166–179. [CrossRef]

125. Chen, Z.-D.; Wang, Y.-G.; Li, L.; Lv, R.-D.; Wei, L.-L.; Liu, S.-C.; Wang, J.; Wang, X. Reduced graphene oxide as saturable absorbers for erbium-doped passively mode-locked fiber laser. *Chin. Phys. B* **2018**, *27*, 084206. [CrossRef]

126. Su, Y.; Huang, X.; Hu, H.; Wen, Y.; Xie, X.; Si, J.; Wang, Y.; Zhao, W. A dual-wavelength Q-switched fiber laser based on reduced graphene oxides. *Laser Phys.* **2019**, *29*, 065101. [CrossRef]

127. Xu, J.; Wu, S.; Liu, J.; Wang, Q.; Yang, Q.H.; Wang, P. Femtosecond Er-doped fiber lasers mode-locked with graphene oxide saturable absorber. In Proceedings of the 2012 Conference on Lasers and Electro-Optics (CLEO), San Jose, CA, USA, 6–11 May 2012; pp. 1–2.

128. Sobon, G.; Sotor, J.; Jagiello, J.; Kozinski, R.; Zdrojek, M.; Holdynski, M.; Paletko, P.; Boguslawski, J.; Lipinska, L.; Abramski, K.M. Graphene Oxide vs. Reduced Graphene Oxide as saturable absorbers for Er-doped passively mode-locked fiber laser. *Opt. Express* **2012**, *20*, 19463–19473. [CrossRef]

129. Cheng, Z.; Xu, J.; Liu, J.; Ren, J.; Wang, P. *Mode-Locked and Q-Switched Fiber Lasers with Graphene Oxide Based Saturable Absorber*; SPIE: Baltimore, MD, USA, 2015; Volume 9466.

130. Li, X.; Wu, K.; Sun, Z.; Meng, B.; Wang, Y.; Wang, Y.; Yu, X.; Yu, X.; Zhang, Y.; Shum, P.P.; et al. Single-wall carbon nanotubes and graphene oxide-based saturable absorbers for low phase noise mode-locked fiber lasers. *Sci. Rep.* **2016**, *6*, 25266. [CrossRef] [PubMed]

131. Gerosa, R.M.; Steinberg, D.; Nagaoka, D.A.; Zapata, J.D.; Domingues, S.H.; Thoroh de Souza, E.A.; Saito, L.A.M. Liquid phase exfoliated black phosphorus and reduced graphene oxide polymer-based saturable absorbers fabrication using the droplet method for mode-locking applications. *Opt. Laser Technol.* **2018**, *106*, 107–112. [CrossRef]

132. García-Córdova, J.Z.; Arano-Martinez, J.A.; Mercado-Zúñiga, C.; Martínez-González, C.L.; Torres-Torres, C. Predicting the Multiphotonic Absorption in Graphene by Machine Learning. *AI* **2024**, *5*, 2203–2217. [CrossRef]

133. Haris, H.; Batumalay, M.; Jin, T.S.; Muhammad, A.R.; Markom, A.M.; Anyi, C.L.; Izani, M.H.; Razak, M.Z.A.; Megat Hasnan, M.M.I.; Saad, I. Ultrafast L Band Soliton Pulse Generation in Erbium-Doped Fiber Laser Based on Graphene Oxide Saturable Absorber. *Crystals* **2023**, *13*, 141. [CrossRef]

134. Abbas, M.; Buntinx, M.; Deferme, W.; Reddy, N.; Peeters, R. Oxygen Gas and UV Barrier Properties of Nano-ZnO-Coated PET and PHBHHx Materials Fabricated by Ultrasonic Spray-Coating Technique. *Nanomaterials* **2021**, *11*, 449. [CrossRef]

135. Kaddoura, M.; Majeau-Bettez, G.; Amor, B.; Poirier, D.; Margni, M. Estimating and reducing dissipative losses in thermal spray: A parametrized material flow analysis approach. *J. Clean. Prod.* **2024**, *450*, 141978. [CrossRef]

136. Muhammad, F.; Zulkifli, M.Z.; Latif, A.; Harun, S.W.; Ahmad, H. Graphene-Based Saturable Absorber for Single-Longitudinal-Mode Operation of Highly Doped Erbium-Doped Fiber Laser. *IEEE Photonics J.* **2012**, *4*, 467–475. [CrossRef]

137. Ahmad, H.; Faruki, M.J.; Razak, M.Z.A.; Tiu, Z.C.; Ismail, M.F. Evanescent field interaction of tapered fiber with graphene oxide in generation of wide-bandwidth mode-locked pulses. *Opt. Laser Technol.* **2017**, *88*, 166–171. [CrossRef]

138. Tosi, D.; Sypabekova, M.; Bekmurzayeva, A.; Molardi, C.; Dukenbayev, K. (Eds.) 4—Tapered and photonic crystal fibers. In *Optical Fiber Biosensors*; Academic Press: Cambridge, MA, USA, 2022.

139. Razalli, S.; Jaddoa, M.; Faruki, M.J.; Razak, M.; Ahmad, H. Passively Q-switched fibre laser based on interaction of evanescent field in optical microfibre with graphene-oxide saturable absorber. *Ukr. J. Phys. Opt.* **2016**, *17*, 58–64.

140. Sahoo, S.K.; Manoharan, B.; Sivakumar, N. *Introduction: Why Perovskite and Perovskite Solar Cells?* Academic Press: Cambridge, MA, USA, 2018.

141. Mikhailov, E.K.; Bobkov, K.K.; Levchenko, A.E.; Velmiskin, V.V.; Khudyakov, D.V.; Aleshkina, S.S.; Zaushitsyna, T.S.; Bubnov, M.M.; Lipatov, D.S.; Likhachev, M.E. Picosecond Pulse Tapered Fiber Amplifier Operated near 1030 nm with Peak Power up to 1 MW. *Photonics* **2023**, *10*, 1385. [CrossRef]

142. Hu, C.; Ma, X.; Wang, C.; Zhou, S.; Wu, H.; Sun, K. High-quality rapid fabrication method of a D-shaped optical fiber based on a CO_2 laser. *Opt. Mater. Express* **2021**, *11*, 2025–2036. [CrossRef]

143. Li, L.; Wang, Y.; Wang, X.; Lv, R.; Liu, S.; Chen, Z.; Wang, J. Generation of dark solitons in Er-doped fiber laser based on ferroferric-oxide nanoparticles. *Opt. Laser Technol.* **2018**, *103*, 354–358. [CrossRef]
144. Ahmad, H.; Soltani, S.; Thambiratnam, K.; Yasin, M.; Tiu, Z.C. Mode-locking in Er-doped fiber laser with reduced graphene oxide on a side-polished fiber as saturable absorber. *Opt. Fiber Technol.* **2019**, *50*, 177–182. [CrossRef]
145. Al-Hiti, A.S.; Al-Masoodi, A.H.H.; Harun, S.W.; Yasin, M.; Wong, W.R. Tungsten trioxide (WO3) film absorber for generating soliton mode-locked pulses in erbium laser. *Opt. Laser Technol.* **2020**, *131*, 106429. [CrossRef]
146. Yunus, Y.; Mahadzir, N.A.; Mohamed Ansari, M.N.; Tg Abd Aziz, T.H.; Mohd Afdzaluddin, A.; Anwar, H.; Wang, M.; Ismail, A.G. Review of the Common Deposition Methods of Thin-Film Pentacene, Its Derivatives, and Their Performance. *Polymers* **2022**, *14*, 1112. [CrossRef]
147. Gerosa, R.M.; Suarez, F.G.; Vianna, P.G.; Domingues, S.H.; de Matos, C.J.S. One-step deposition and in-situ reduction of graphene oxide in photonic crystal fiber for all-fiber laser mode locking. *Opt. Laser Technol.* **2020**, *121*, 105838. [CrossRef]
148. Mansoor, A.K.W.; Hamida, B.A.; Eltaif, T.; Ismail, E.I.; Kadir, N.A.A.; Khan, S.; Harun, S.W. Passively Q-switched Erbium-Doped Fiber Laser based on Graphene Oxide as Saturable Absorber. *J. Opt. Commun.* **2018**, *39*, 307–310. [CrossRef]
149. Harun, S.W.; Haris, H. Soliton pulses generation with graphene oxide saturable absorber. In *Optical Fiber Laser Technology*; Penerbit UTHM: Batu Pahat, Malaysia, 2020; pp. 1–12.
150. Chen, H.-R.; Tsai, C.-Y.; Cheng, H.-M.; Lin, K.-H.; Hsieh, W.-F. Passive mode locking of ytterbium- and erbium-doped all-fiber lasers using graphene oxide saturable absorbers. *Opt. Express* **2014**, *22*, 12880–12889. [CrossRef]
151. He, X.; Liu, Z.-B.; Wang, D.N.; Yang, M.; Liao, C.R.; Zhao, X. Passively Mode-Locked Fiber Laser Based on Reduced Graphene Oxide on Microfiber for Ultra-Wide-Band Doublet Pulse Generation. *J. Light. Technol.* **2012**, *30*, 984. [CrossRef]
152. Zhao, J.Q.; Wang, Y.G.; Yan, P.G.; Ruan, S.C.; Cheng, J.Q.; Du, G.G.; Yu, Y.Q.; Zhang, G.L.; Wei, H.F.; Luo, J.; et al. Graphene-Oxide-Based Q-Switched Fiber Laser with Stable Five-Wavelength Operation. *Chin. Phys. Lett.* **2012**, *29*, 114206. [CrossRef]
153. Xu, J.; Wu, S.; Li, H.; Liu, J.; Sun, R.; Tan, F.; Yang, Q.-H.; Wang, P. Dissipative soliton generation from a graphene oxide mode-locked Er-doped fiber laser. *Opt. Express* **2012**, *20*, 23653–23658. [CrossRef] [PubMed]
154. Zaca-Morán, P.; Gomez, C.L.; Morán, O.Z.; Ortega-Mendoza, J.G.; Pola-López, E.S. Short-pulsed Q-switched fiber laser using graphene oxide quantum dots based as saturable absorber. *Heliyon* **2023**, *9*, e20136. [CrossRef] [PubMed]
155. Aziz, N.A.; Ahmad, F.; Lokman, M.; Harun, S.W.; Hanafi, E. Generation of Passive Q-switched by using Graphene Oxide in Erbium Doped Fiber Laser. In Proceedings of the 2021 IEEE 19th Student Conference on Research and Development (SCOReD), Kota Kinabalu, Malaysia, 23–25 November 2021.
156. Kim, B.; Hong, S.; Park, J.; Lee, Y.; Yeom, D.-i.; Oh, K. Laser-driven self-exfoliation of graphene oxide layers on a fiber facet for Q switching of an Er-doped fiber laser at the longest wavelength. *Photonics Res.* **2020**, *8*, 1324–1332. [CrossRef]
157. Tiu, Z.C.; Ahmad, F.; Tan, S.J.; Ahmad, H.; Harun, S.W. Passive Q-switched Erbium-doped fiber laser with graphene–polyethylene oxide saturable absorber in three different gain media. *Indian J. Phys.* **2014**, *88*, 727–731. [CrossRef]
158. Yap, Y.; Ming, H.; Harun, S.W.; Ahmad, H. Graphene Oxide-Based Q-Switched Erbium-Doped Fiber Laser. *Chin. Phys. Lett.* **2013**, *30*, 024208. [CrossRef]
159. Ahmad, H.; Muhammad, F.D.; Zulkifli, M.Z.; Harun, S.W. Graphene-Oxide-Based Saturable Absorber for All-Fiber Q-Switching with a Simple Optical Deposition Technique. *IEEE Photonics J.* **2012**, *4*, 2205–2213. [CrossRef]
160. Mei, C.; Duan, L.; Chang, S.; Guo, X.; Yu, J. Generation of a vector conventional soliton via a graphene oxide saturable absorber. *Appl. Opt.* **2023**, *62*, 5394–5398. [CrossRef]
161. Tsai, L.-Y.; Li, Z.-Y.; Lin, J.-H.; Song, Y.-F.; Zhang, H. Wavelength tunable passive-mode locked Er-doped fiber laser based on graphene oxide nano-platelet. *Opt. Laser Technol.* **2021**, *140*, 106932. [CrossRef]
162. Haris, H.; Harun, S.W.; Yupapin, P.; Arof, H.; Apsari, R. Generation of Vector Soliton Pulses with Graphene Oxide Film in Mode-locked Erbium-doped Fiber Laser Cavity. *Nonlinear Opt. Quantum Opt.* **2020**, *52*, 111–118.
163. Haris, H.; Harun, S.; Muhammad, A.; Arof, H. Graphene oxide-polyethylene oxide (PEO) film as saturable absorber on mode-locked erbium doped fiber laser generation. *J. Teknol.* **2016**, *78*. [CrossRef]
164. Ismail, M.A.; Ahmad, H.; Harun, S.W. Soliton Mode-Locked Erbium-Doped Fiber Laser Using Non-Conductive Graphene Oxide Paper. *IEEE J. Quantum Electron.* **2014**, *50*, 85–87. [CrossRef]
165. Xu, J.; Liu, J.; Wu, S.; Yang, Q.-H.; Wang, P. Graphene oxide mode-locked femtosecond erbium-doped fiber lasers. *Opt. Express* **2012**, *20*, 15474–15480. [CrossRef] [PubMed]